Structure of the ϕ photoproduction amplitude at a few GeV

A. I. Titov,[1,2,*] T.-S. H. Lee,[3,†] H. Toki,[1,‡] and O. Streltsova[2]
[1]*Research Center for Nuclear Physics, Osaka University, Osaka 567-0047, Japan*
[2]*Bogoliubov Laboratory of Theoretical Physics, JINR, Dubna 141980, Russia*
[3]*Physics Division, Argonne National Laboratory, Illinois 60439*
(Received 8 March 1999; published 29 July 1999)

The structure of the ϕ photoproduction amplitude in the $\sqrt{s}\sim 2-5$ GeV region is analyzed based on Pomeron-exchange and meson-exchange mechanisms. The SU(3) symmetry and the ϕ decay widths are exploited to determine the parameters that are needed to predict the amplitudes due to pseudoscalar mesons (π^0,η) exchange, scalar mesons (σ,a_0,f_0) exchange, and the ϕ radiation from the nucleon. In addition to the universally accepted Pomeron exchange with an intercept $\alpha(0)\sim 1.08$, we investigate the role of a second Pomeron with $\alpha(0)<0$, as inspired by the glueball $(J^\pi=0^+, M_b^2\sim 3\ \mathrm{GeV}^2)$ predicted by the lattice QCD calculation and dual Ginsburg-Landau model. It is found that the existing limited data at low energies near threshold can accommodate either the second Pomeron or the scalar mesons exchange. The differences between these two competing mechanisms are shown to have profound effects on various density matrices which can be used to calculate the cross sections as well as various single and double polarization observables. We predict a definite isotopic effect: polarization observables of ϕ photoproduction on the proton and neutron targets can have differences of a factor 2 and more. [S0556-2813(99)04908-0]

PACS number(s): 25.20.Lj, 13.60.Le, 21.30.Cb

I. INTRODUCTION

The investigation of the reaction $\gamma p\to\phi p$ is interesting for several reasons. Traditionally, it is considered as a tool for the study of the Pomeron exchange dynamics, implying that (i) the vector meson dominance model (VDM) [1–9] is valid and (ii) the other hadronic channels are suppressed by the OZI rule. This mechanism is depicted schematically in Fig. 1(a). It is fairly well established that the $\gamma p\to\phi p$ data at high energies can be described by a Pomeron trajectory with an intercept $\alpha(0)=1.08$ [2–6]. At low energies $\sqrt{s}<5$ GeV, the predictions based on this Pomeron trajectory appear to be lower than the existing limited data. It has been suggested that this discrepancy indicates the existence of more exotic mechanisms corresponding to additional trajectories including the glueball trajectory [10].

Another interesting subject is related to the strange degrees of freedom. Since the ϕ meson is thought to consist mainly of strange quarks, i.e., $s\bar{s}$, with a rather small contribution of the light u,d quarks, its production should be suppressed if the entrance channel does not possess a considerable admixture of strangeness. Indeed, the recent experiments on the proton annihilation at rest (see Ref. [11] for references and a compilation of data) point to a large apparent violation of the OZI rule, which is interpreted [11] as a hint to an intrinsic $s\bar{s}$ component in the proton. However, the data can be explained by modifying meson exchange models [12] without introducing any strangeness component in the nucleon or OZI-violation mechanisms. On the other hand, the analysis of the πN σ term [13] suggests that the proton might contain a strange quark admixture as large as 20%. Thus this issue remains controversial. Therefore it is tempting to look for other observables [11,14,15] that are directly related to the strangeness content of the nucleon. The use of ϕ photoproduction has been considered as one of the most promising approaches. Through the interference with the ''nonstrange'' amplitude, it is shown in Ref. [15] that polarization observables of the ϕ photoproduction are sensitive even to a rather small strangeness admixture in the proton. Obviously, reliable information about the hidden strangeness manifestation in the ϕ photoproduction can be obtained only when the nonstrange amplitude has been understood quantitatively. This is the objective of this work.

The nonstrange amplitude is due to the diffractive Pomeron exchange, meson exchange, and direct ϕ radiation from nucleons. They are illustrated in Fig. 1. The pseudoscalar mesons (PSE) π and η are expected to be most relevant in determining the meson exchange term Fig. 1(b). However, the calculation of the η exchange involves the coupling constant $g_{\eta NN}$ which is not well determined experimentally. For the ϕ-radiation term [Fig. 1(c)], we have the same problem with ϕNN vector and tensor couplings. Nevertheless, these parameters can be estimated theoretically by imposing SU(3) symmetry. For example, the finite ϕNN coupling constants can be estimated by considering the $\phi\pi\rho$

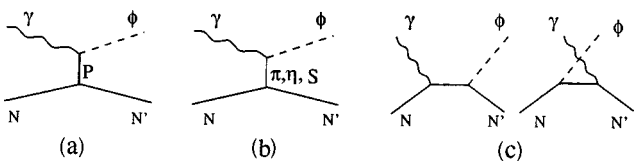

FIG. 1. Diagrammatic representations of processes of the ϕ production: (a) diffractive Pomeron exchange photoproduction, (b) photoproduction with boson exchange, and (c) ϕ meson emission from the nucleon legs.

*Electronic address: atitov@thsun1.jinr.ru
†Electronic address: lee@anph09.phy.anl.gov
‡Electronic address: toki@rcnp.osaka-u.ac.jp

couplings and the interaction of the ϕ meson with the kaon cloud of nucleon [16].

We also consider the scalar meson exchange (SE) for Fig. 1(b). In ω photoproduction, VDM predicts some relative suppression of SE as compared with PSE, proportional to g_ρ^2/g_ω^2, where g_V^{-1} is the electromagnetic strength of the vector meson [17]

$$J_\mu^V = \frac{eM_V^2}{2g_V} V_\mu, \tag{1}$$

which can be found from the e^+e^- partial decay width of ρ/ω mesons. In Eq. (1) M_V is the mass of the vector meson. So, the relative suppression of SE/PSE for unpolarized cross section is proportional to $g_\rho^2/g_\omega^2 \simeq 11.5^{-1}$ [18], which is in agreement with the SU(3) flavor prediction $g_\rho : g_\omega : g_\phi = 1/3 : 1 : 1/\sqrt{2}$. For ϕ photoproduction the ratio g_ρ^2/g_ϕ^2 increases by a factor 2, and taking into account several known candidates for SE, one expects that their coherent contribution may be comparable with the other discussed mechanisms.

A step towards an understanding of the structure of the ''nonstrange'' background in ϕ photoproduction was taken in a recent paper [19]. The focus of Ref. [19] is to explore the possibility of determining the ϕNN and ηNN coupling constants using the $\gamma p \to \phi p$ reaction. The scalar mesons exchange is not considered. Except the πNN coupling constant, all parameters associated with Pomeron exchange, η exchange, and direct ϕ-radiation amplitudes are adjusted to fit the data. In this paper we take a different approach. We calculate the pseudoscalar meson exchange, and the direct ϕ-radiation amplitudes using the parameters *predetermined* by using SU(3) symmetry and ϕ decay widths. This will allow us explore the parameters associated with the scalar meson exchange, and the second Pomeron trajectory that will be introduced later.

In this work we give a systematical analysis of ϕ photoproduction in a few GeV region where the interferences between the three mechanisms depicted in Fig. 1 are essential. We focus on the diffractive Pomeron exchange and scalar meson exchange which are not well defined in this low energy region. This is done by analyzing three models. The first one (model A) consists of the π, η exchange amplitude and the standard Pomeron (P_1) exchange that has been determined at high energies in many works (see Refs. [1–6,15]). In the second case (model B), we extend model A to include the second Pomeron exchange (P_2) inspired by the ($J^\pi = 0^+, M_b^2 \sim 3\ \mathrm{GeV}^2$) glueball predicted by the lattice QCD calculation and dual Ginsburg-Landau model. The third model (model C) is to extend model A to include scalar meson exchange. The most important difference between models B and C is that the phase of P_2 at forward angle $\theta = 0$ is complex as defined by the Regge phenomenology, while the phase of scalar exchange is fixed by the Feynman rules and is real. It is therefore natural to expect that their differences can be best investigated by considering polarization observables.

In Sec. II, we define the kinematical variables and formula for calculating cross section and polarization observables. The basic amplitudes for mechanisms illustrated in Fig. 1 will be given explicitly in Sec. III. The parameters for PSE amplitudes will also be given there. Section IV is devoted to the unpolarized cross section, with which we fix the parameters of the Pomeron exchange for the considered three models. The result for the spin density matrix elements together with discussion of the main peculiarities in K^+K^- angular distribution is given in Sec. V. In Sec. VI we analyze the beam target and beam recoil-nucleon asymmetries for proton and neutron targets. The summary is given in Sec. VII. The appendixes are given to describe the general formalism of the ϕ decay angular distribution, discuss the relative phases $\phi \to \gamma\pi, \eta$ decays, and fix the parameters of the scalar exchange amplitude.

II. OBSERVABLES

We define the kinematical variables for the $\gamma + N \to \phi + N$ reaction using the standard notation. The four-momenta of the incoming photon, outgoing ϕ, initial (target) nucleon, and final (recoil) nucleon are k, q, p, and p', respectively. These variables in the center-of-mass system (c.m.s.) are written as $k = (\nu, \mathbf{k})$, $q = (E_\phi, \mathbf{q})$, $p = (E_p, -\mathbf{k})$, and $p' = (E_{p'}, -\mathbf{q})$. Hereafter θ denotes the ϕ production angle in c.m.s., $t = (p - p')^2 = (q - k)^2$ and $s \equiv W^2 = (p + k)^2$, M_N is the nucleon mass, M_π is the pion mass, M_ϕ is the ϕ mass, etc. We use the conventions of Bjorken and Drell to define the γ matrices and Dirac spinors.

The cross section in c.m.s. is related to the invariant amplitude T_{fi} as

$$d\sigma_{fi} = \frac{M_N^2}{2\pi^2 (W^2 - M_N^2)} |T_{fi}|^2 \frac{d\mathbf{p}'}{2E_{p'}} \frac{d\mathbf{q}}{2E_\phi} \delta^4(p + k - p' - q). \tag{2}$$

The corresponding unpolarized differential cross section is given by

$$\frac{d\sigma_{fi}}{dt} = \frac{M_N^2}{4\pi (W^2 - M_N^2)^2} \overline{|T_{fi}|^2}, \tag{3}$$

with

$$\overline{|T_{fi}|^2} = \frac{1}{4} \sum_{\lambda_i, \lambda_f, \lambda_\gamma, \lambda_\phi} |T_{\lambda_f, \lambda_\phi; \lambda_i, \lambda_\gamma}|^2, \tag{4}$$

where $\lambda_i, \lambda_\gamma$ are the helicities of the incoming nucleon and photon, and λ_f, λ_ϕ are the helicities of the outgoing nucleon and ϕ. Note that Eq. (3) has no ''threshold'' factor ($|\mathbf{q}|/|\mathbf{k}|$) which is used sometimes in extrapolating formulas in the near threshold energy region $s \to s_{\mathrm{th}} = (M_N + M_\phi)^2$, where $|\mathbf{q}| \to 0$. This means that near the threshold the differential cross section $d\sigma/dt$ may be finite, contrary to $d\sigma/d\Omega$, which is proportional to $|\mathbf{q}|$ and vanishes at $s \to s_{\mathrm{th}}$.

For experimental tests of our predictions, it is most convenient to present the quantities that are directly related to the angular distributions of the $\phi \to K^+K^-$ in the ϕ rest

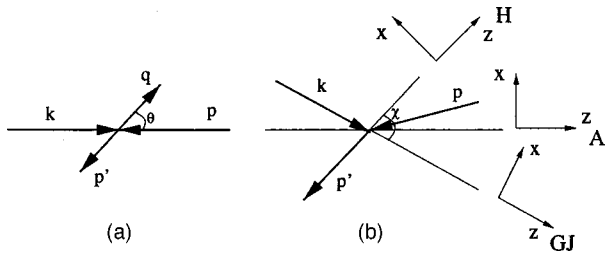

FIG. 2. Diagrammatic representations of (a) the center-of-mass system and (b) the ϕ meson rest frame. The labels H, GJ, and A correspond to helicity, Gottfried-Jackson, and Adair reference systems, respectively.

frame where $\mathbf{q}_\phi = 0$. Figures 2(a), 2(b) schematically depict the c.m.s. and the ϕ rest frames, respectively, in the ϕ production plane. The **Y** axis is perpendicular to the production plane: $\mathbf{Y} = \mathbf{p} \times \mathbf{p}' / |\mathbf{p} \times \mathbf{p}'|$. There are several choices of the quantization axis **Z**: the ϕ-meson helicity system (H) with **Z** opposite to the direction of the recoiling nucleon, the Gottfried-Jackson (GJ) system with **Z** parallel to the momentum of the photon, and the Adair (A) system with **Z** parallel to the photon momentum in c.m.s. It is difficult to give a priority to one of these systems first. Some qualitative considerations presented in Appendix A are in favor of the Gottfried-Jackson system, because certain amplitudes in this frame take a simple helicity conserving form for an arbitrary ϕ production angle θ. Although the general formalism for the analysis of the ϕ decay does not depend on the system, all our concrete calculations are done in GJ system.

Thus, the decay angles Θ, Φ are defined as the polar and the azimuthal angles of the direction of one of the decay particles in the ϕ-meson rest frame. The angular distribution of $\phi \to a + b$ decay is then defined by

$$\frac{dN}{d\cos\Theta d\Phi} = \sum |T_{\lambda_f,\lambda_\phi;\lambda_i,\lambda_\gamma} \cdot M_{\lambda_\phi}(\Theta,\Phi)|^2, \qquad (5)$$

where the decay amplitude reads

$$M_{\lambda_\phi}(\Theta,\Phi) = C_0 \sqrt{\frac{3}{4\pi}} D^{1*}_{\lambda_\phi \lambda_{ab}}(\Phi,\Theta,-\Phi), \qquad (6)$$

with $\lambda_{ab} \equiv \lambda_a - \lambda_b$, where $\lambda_{a(b)}$ is the helicity of $a(b)$. The constant $|C_0|^2$ is proportional to the decay width and if we are working with normalized angular distributions it drops out of the final result, so we can set $C_0 = 1$. Using Eq. (5) one can express the normalized distribution in the following form:

$$\frac{d\mathcal{N}}{d\cos\Theta d\Phi} \equiv \mathcal{W}(\cos\Theta,\Phi) = \frac{3}{4\pi} \sum_{\lambda,\lambda'} D^{1*}_{\lambda\lambda_{ab}}(\Phi,\Theta,-\Phi) \rho_{\lambda\lambda'} \times D^{1}_{\lambda'\lambda_{ab}}(\Phi,\Theta,-\Phi), \qquad (7)$$

where $\rho_{\lambda\lambda'}$ is the ϕ spin density matrix

$$\rho_{\lambda\lambda'} = \frac{1}{N} \sum_{\lambda_f,\lambda_\gamma,\lambda_i,\lambda'_\gamma} T_{\lambda_f\lambda;\lambda_i\lambda_\gamma} \rho(\gamma)_{\lambda_\gamma\lambda'_\gamma} T^*_{\lambda_f\lambda';\lambda_i\lambda'_\gamma}. \qquad (8)$$

The normalization N factor reads

$$N = \sum |T_{\lambda_f\lambda;\lambda_i\lambda_\gamma}|^2. \qquad (9)$$

The matrix $\rho(\gamma)_{\lambda_\gamma\lambda'_\gamma}$ is the incoming photon density matrix.

In this work we make predictions for the cases that the incident photons are either circularly polarized or linearly polarized. The corresponding ''partial'' distribution functions $W^\alpha(\cos\Theta,\Phi)$ have been well described in the literature (see Ref. [20]). For completeness and the discussions of our results, the derivation of these polarization quantities will be given in Appendix A. It is shown that by appropriately combining these distribution functions, some ϕ density matrices $\rho^\alpha_{\lambda,\lambda'}$ and asymmetry observables Σ_ϕ and P_σ can be extracted directly from the data. We will also discuss their physical meaning.

More complicated and, in general, more informative observables may be obtained when we include ''target'' or ''recoil'' spins into considerations. For example, the derivations outlined in Appendix A can be straightforwardly generalized to obtain formula for the polarized target if we leave out the summation on the proton helicity λ_i in Eq. (8) and fix it according to the experimental condition. However, such quantities involve triple coincident measurements which are difficult to perform.

An easier experiment is to only measure the double polarization observables in the beam-target (recoil) sector without fixing decay angular distribution. We will consider some of them, using the notation of Ref. [21]. All of them are given in c.m.s. The beam-target asymmetry is

$$C^{\mathrm{BT}}_{zz} = -\frac{\sum |T_{\lambda_f,\lambda_\phi;1/2,1} - T_{\lambda_f,\lambda_\phi;-1/2,1}|^2}{\sum |T_{\lambda_f,\lambda_\phi;1/2,1} + T_{\lambda_f,\lambda_\phi;-1/2,1}|^2} = \frac{d\sigma(3/2) - d\sigma(1/2)}{d\sigma(3/2) + d\sigma(1/2)}, \qquad (10)$$

where $\frac{3}{2}, \frac{1}{2}$ stand for the values of the total spin in the initial state. The beam-recoil asymmetry $(\mathbf{zx}')$, where $\mathbf{x}'$ along the vector $[\boldsymbol{k} \times \boldsymbol{q}] \times \boldsymbol{q}$ is

$$C^{BR}_{zx'} = -2\frac{\sum \mathrm{Re}\, T_{1/2,\lambda_\phi;\lambda_i,1} T^*_{-1/2,\lambda_\phi;\lambda_i,1}}{\sum |T_{\lambda_f,\lambda_\phi;\lambda_i,1}|^2} = -\frac{d\sigma(x') - d\sigma(-x')}{d\sigma(x') + d\sigma(-x')}, \qquad (11)$$

where $d\sigma(\pm x')$ stands for the cross section with the recoil proton polarization along or opposite to $\boldsymbol{x}'$ axis.

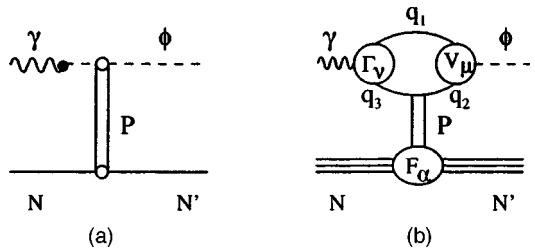

FIG. 3. Diagrammatic representation of the Pomeron exchange model for ϕ photoproduction: (a) VDM model and (b) the corresponding quark diagram in the Donnachie and Landshoff model.

III. BASIC AMPLITUDES

A. Pomeron exchange amplitudes

In the vector meson dominance model (VDM) [22,23], the incoming photon first converts into a vector meson which then scatters diffractively from the nucleon through the Pomeron exchange, as shown in Fig. 3(a). Experimental data for vector-meson photoproduction, small-$|t|$ hadron-hadron elastic scattering, and diffractive electrodissociation indicate that Pomeron behaves rather similar to a $C=+1$ isoscalar photon [1,2]. It can be shown that the data at high energies can be described by a Pomeron trajectory with an intercept $\alpha(0)\sim 1.08$. This trajectory will be called the P_1 trajectory in this paper. Within Regge theory, it is easily to see that the P_1 trajectory can only be identified with objects with spin $J>0$. It was suggested [10] that a different Pomeron trajectory, as inspired by the glueball ($J^\pi=0^+$, $M^2_{\rm gb}\simeq 3$ GeV) predicted by lattice QCD calculations and a QCD-based dual Ginsburg-Landau model [24], could dominate the cross section at low energies by having a negative intercept $\alpha(0)$. This Pomeron trajectory, called P_2, will be also considered in this work.

Within QCD, a microscopic model of Pomeron exchange was proposed by Donnachie and Landshoff [3] (DL model). It is assumed that the incoming photon first converts into a quark-antiquark pair, which then exchanges a Pomeron with the nucleon before recombining into an outgoing ϕ meson, as depicted in Fig. 3(b). The DL model was examined in Ref. [2] by using a Euclidean QCD model of mesons to evaluate exactly the quark-loop integration in Fig. 3(b). It was shown that the interpretation of the Pomeron as gluonic object is consistent with the data up to very large Q^2 and W. For the $Q^2=0$ and $W<5$ GeV region considered in this work, the exact loop integration, as done in Ref. [2], can be approximated by the factorized form employed by Donnachie and Landshoff. We therefore follow Donnachie and Landshoff and use this simplified version of the model to define the Pomeron-exchange amplitudes. We will not consider two-gluon-exchange models of the Pomeron as proposed in Refs. [4–6].

Within the factorized form of the DL model, the invariant amplitude can be written as

$$T^{P_n}_{fi}=\bar{u}_{m_f}(p')M^{P_n}_0\varepsilon^*_{\phi\mu}\mathcal{M}^{P_n\mu\nu}\varepsilon_{\gamma\nu}u_{m_i}(p), \tag{12}$$

with

$$\mathcal{M}^{P_n\mu\nu}=\mathcal{F}^{P_n}_\alpha\Gamma^{P_n\alpha,\mu\nu}. \tag{13}$$

Here $u(p)$ is the Dirac spinor, $\varepsilon_{\gamma\nu}$ and $\varepsilon_{\phi\mu}$ are respectively the polarization vectors of the photon and ϕ meson, $\mathcal{F}^{P_n}_\alpha$ describes the Pomeron-nucleon vertex, and $\Gamma^{P_n\alpha,\mu\nu}$ is associated with the Pomeron–vector-meson coupling which is related to the $\gamma\to q\bar{q}$ vertex Γ_ν and the $q\bar{q}\to\phi$ vertex V_μ, as shown in Fig. 3(b). We follow the DL model and assume that the P_1-nucleon coupling is photonlike. For the P_2-nucleon vertex, we assume a scalar coupling. Accordingly, we have

$$\mathcal{F}^{P_1}_\alpha=\gamma_\alpha, \tag{14}$$

$$\mathcal{F}^{P_2}_\alpha=1. \tag{15}$$

An explicit evaluation [21] of the Dirac algebra associated with the quark-loop shown in Fig. 3(b) leads to the following form of the Pomeron-vector meson coupling in Eq. (13):

$$\Gamma^{P_1\alpha,\mu\nu}=g^{\alpha\nu}k^\mu-k^\alpha g^{\mu\nu},$$

$$\Gamma^{P_2\mu\nu}=(k^\mu q^\nu-k\cdot q g^{\mu\nu})/M_\phi, \tag{16}$$

where the transversality conditions $\mathcal{M}^{P_{1,2}\mu\nu}\cdot q_\mu=\mathcal{M}^{P_{1,2}\mu\nu}\cdot k_\nu=0$ are fulfilled. The strength factors $M^{P_{1,2}}_0$ in Eq. (12) take the conventional form of Regge parametrization

$$M^{P_i}_0=C_iF(t)F_i(s,t)e^{-i(\pi/2)\alpha_i(t)}\left(\frac{s-s_i}{s_0}\right)^{\alpha_i(t)}, \tag{17}$$

where the trajectories are taken to be

$$\alpha_1(t)=\alpha_1(0)+\alpha_1' t=1.08+0.25t,$$

$$\alpha_2(t)=-0.75+0.25t, s_0=\alpha'^{-1}. \tag{18}$$

As discussed above, $\alpha_1(t)$ is chosen to fit the data at large s and $\alpha_2(t)$ is inspired by the ($J^\pi=0^+$, $M^2_{\rm gb}\sim 3$ GeV^2) glueball, predicted by Lattice QCD calculations and a QCD-based Dual Landau-Ginsburg model [24]. We follow Ref. [7] to define the overall form factor in Eq. (17) as $F(t)=F_\phi(t)\cdot F_N(t)$ with

$$F_N(t)=(4M_N^2-2.8t)/\{(4M_N^2-t)[1-(t/0.7)]^2\},$$

$$F_\phi(t)=\exp\left[\frac{1}{2}B(t-t_{\rm max})\right]. \tag{19}$$

The correcting functions $F_{1,2}(s,t)$ for Eq. (17) are

$$F_i^{-2}=\frac{1}{4}\Gamma^{P_i\alpha}_{\mu\nu}\Gamma^{P_i\alpha'}_{\mu'\nu'}\,{\rm Tr}\{g^{P_i}_\alpha(\not{p}+M_N)g^{P_i}_{\alpha'}(\not{p}'+M_N)\}$$

$$\times(g^{\mu\mu'}-q^\mu q^{\mu'}/M^2_\phi)g^{\nu\nu'}/4M_N^2, \tag{20}$$

and explicitly read

$$F_1^{-2}=\frac{1}{2M_N^2M_\phi^2}\{k\cdot p[k\cdot pM_\phi^2+(k\cdot q)^2]+2k\cdot pk\cdot q[p\cdot q-M_\phi^2]-(k\cdot q)^2[p\cdot q+M_N^2]\},$$

$$F_2^{-2}=\frac{1}{2M_N^2M_\phi^2}(k\cdot q)^2(p\cdot(k-q)+2M_N^2). \quad (21)$$

The strength factor C_1 in Eq. (17) is chosen to reproduce $d\sigma/dt|_{\theta=0}$ at large s, where the cross section is entirely due to P_1 trajectory. The strength factor C_2 is chosen to reproduce $d\sigma/dt|_{\theta=0}$ at low energies where all mechanisms shown in Fig. 1 are important. The slope B is chosen to reproduce the available data of angular distributions $d\sigma/dt$. Note that the phase of the Pomeron exchange amplitudes is fixed and controlled by the exponential factors in Eq. (17). At $t=0$, the real part of P_1 amplitude almost vanishes, while the P_2 amplitude remains complex.

B. Pseudoscalar exchange amplitudes

To calculate the pseudoscalar meson ($\phi=\pi^0,\eta$) exchange, we follow the previous investigations (see Refs. [18,19,21,25]) and assume that the effective Lagrangian for the $\phi\gamma\varphi$ with $\varphi=\pi^0,\eta$ interaction has the following form:

$$\mathcal{L}_{\phi\gamma\varphi}=\frac{e}{M_\phi}g_{\phi\gamma\varphi}\epsilon^{\mu\nu\alpha\beta}\partial_\mu\phi_\nu\partial_\alpha A_\beta\varphi, \quad (22)$$

where A_β is the photon field. For the $NN\varphi$ interaction, one can use either pseudoscalar or pseudovector coupling which are equivalent at the tree level. For definiteness we use the pseudovector coupling of the form

$$\mathcal{L}_{PS}=\frac{g_{\pi^0NN}}{2M_N}\bar{N}\gamma_\mu\gamma_5N\partial^\mu\pi^0+\frac{g_{\eta NN}}{2M_N}\bar{N}\gamma_\mu\gamma_5N\partial^\mu\eta. \quad (23)$$

The one-meson-exchange amplitude then takes the following factorized form:

$$T_{fi}^{\rm PSE}=\frac{-i}{t-M_\varphi^2}\ \frac{e}{M_\phi}g_{\varphi NN}g_{\phi\gamma\varphi}W^F_{m_f,m_i}W^B_{\lambda_\phi,\lambda_\gamma}, \quad (24)$$

where

$$W^F_{m_f,m_i}=\bar{u}_{m_f}(p')\gamma_5u_{m_i}(p),$$

$$W^B_{\lambda_\phi,\lambda_\gamma}=\epsilon^{\mu\nu\alpha\beta}q_\mu k_\alpha\varepsilon_{\phi\nu}\varepsilon_{\gamma\beta}. \quad (25)$$

Direct calculation of W^F and W^B in the center-of-mass frame gives

$$W^F_{m_f,m_i}=C\{2m_f[\alpha(p')\cos\theta-\alpha(p)]\times\delta_{m_fm_i}-\alpha(p')\sin\theta\delta_{m_f-m_i}\},$$

$$W^B_{\lambda_\phi,\lambda_\gamma}=iE_\gamma\Big[\lambda_\gamma(E_\phi-|\mathbf{q}|\cos\theta)\boldsymbol{\varepsilon}_\phi\cdot\boldsymbol{\varepsilon}_\gamma+\frac{|\mathbf{q}|\sin\theta}{\sqrt{2}M_\phi}(|\mathbf{q}|-E_\phi\cos\theta)\delta_{\lambda_\phi0}-\frac{\lambda_\phi|\mathbf{q}|\sin^2\theta}{2}\Big], \quad (26)$$

where $m_{i,f}$ is the nucleon spin projection, $C=\sqrt{(E_p+M_N)(E_{p'}+M_N)}/2M_N$ and $\alpha(p)=\sqrt{(E_p-M_N)/(E_p+M_N)}$.

In the ϕ meson rest frame ($\boldsymbol{q}=0$) the amplitude takes the very simple form

$$T_{fi}^{\rm PSE}=(2m_i\lambda_\gamma)\boldsymbol{\varepsilon}_\phi\cdot\boldsymbol{\varepsilon}_\gamma T_{0fi}^{\rm PSE}, \quad (27)$$

where

$$T_{0fi}^{\rm PSE}=\frac{2m_iM_\phi E_\gamma}{t-M_\varphi^2}\ \frac{e}{M_\phi}g_{\varphi NN}g_{\phi\gamma\varphi}W^F_{m_f,m_i}. \quad (28)$$

We then can see that in the GJ frame the separate form of the amplitude Eq. (27) leads to the spin-conserving form Eq. (A32). Note also that the PSE amplitude is purely real. We now specify the parameters for evaluating the above PSE amplitudes.

(i) $NN\varphi$ vertex. For πNN vertex, the value $g_{\pi NN}=13.39\pm0.08$ was determined in Ref. [26]. In recent analyses, a lower value $g_{\pi NN}\sim13.28$ is recommended [27]. Which value we should use in the present work is related to the form of the associated πNN form factor (discussed below). In this work, we follow the study of ω photoproduction in Ref. [18] and use $g_{\pi NN}=13.26$ and the form factor determined there (no error was assigned in Ref. [18]). This value is within the known experimental error, but still should be considered as part of the phenomenological meson-exchange model employed in Ref. [18] and the present investigation. The status of $NN\eta$ coupling is not so clear. The coupling constant $g^2_{\eta NN}/4\pi$ varies between 0 and 7 in literature. The large value comes from the one boson exchange potentials (cf. Bonn potential [28]), where, however, η exchange gives relatively small effect in fitting the NN scattering phase shift. But most of other studies [28–32] favor a small value for the $NN\eta$ coupling.

In our calculation, we use the value determined by using the SU(3) flavor symmetry. We then have the following relation:

$$g_{\eta NN}=\frac{1}{\sqrt{3}}\ \frac{3F-D}{F+D}g_{\pi NN}, \quad (29)$$

where D and F denote the two different SU(3) octet meson baryon coupling constants. By using the most recent empirical value $F/D=0.575\pm0.016$ [30], we obtain

$$\frac{g^2_{\eta NN}}{4\pi}=0.99\pm0.13. \quad (30)$$

For definiteness, we set $g^2_{\eta NN}/4\pi = 0.99$ in all of our calculations. This value is close to the average of the empirical values determined from the analyses of the NN forward dispersion relation [31] and the other approaches [32–35]. Later, we will discuss separately the dependence of the important polarization observable ϕ decay asymmetry Σ_ϕ on this parameter.

(ii) $\phi\gamma\varphi$ vertex. The effective coupling constant $g_{\phi\gamma\varphi}$ is related to the decay width of $\phi\to\gamma\varphi$, namely,

$$\Gamma(\phi\to\gamma\varphi) = \frac{\alpha}{24}\,\frac{(M_\phi^2 - M_\varphi^2)^3}{M_\phi^5} g^2_{\phi\gamma\varphi}. \tag{31}$$

Using the most recent data

$$\Gamma(\phi\to\gamma\pi^0) = (5.80\pm 0.58)\times 10^{-6}\,\text{GeV},$$

$$\Gamma(\phi\to\gamma\eta) = (5.56\pm 0.26)\times 10^{-5}\,\text{GeV}, \tag{32}$$

we get $|g_{\phi\gamma\pi}| = 0.141\pm 0.007$ and $|g_{\phi\gamma\eta}| = 0.707\pm 0.017$, respectively. One can see that the relatively large $g_{\phi\gamma\eta}$ in the η-exchange amplitude is compensated by the small ηNN coupling constant. Hence the η-exchange and π-exchange amplitudes are comparable and they may interfere strongly with each other. Clearly, it is necessary to make an accurate choice of their phases. In the Appendix B we fix their phases by using the SU(3) symmetry and the results from the previous investigations of pion photoproduction. We find that $g_{\phi\gamma\pi} = -0.141$ and $g_{\phi\gamma\eta} = -0.707$ with respect to the sign of the $\omega\to\gamma\pi$ coupling. Since $g_{\pi^0 pp}$ and $g_{\eta pp}$ is of the same sign within SU(3), we expect *constructive* interference between π and η exchange amplitudes for the $\gamma p\to\phi p$ process. The situation changes in the $\gamma n\to\phi n$ reaction. In this case the isospin property results $g_{\pi^0 nn} = -g_{\pi^0 pp}$, while $g_{\eta nn} = g_{\eta pp}$, and the corresponding interference becomes *destructive*. This striking isospin-dependence effect has been reported in Ref. [37] and will be studied in more detail here.

All vertices in the meson-exchange amplitude [Fig. 1(b)] must be regularized by appropriate form factors. We choose the standard form

$$F_{\varphi NN}(t) = \frac{\Lambda_\varphi^2 - M_\varphi^2}{\Lambda_\varphi^2 - t}, \quad F_{\phi\gamma\varphi}(t) = \frac{\Lambda_{\phi\gamma\varphi}^2 - M_\varphi^2}{\Lambda_{\phi\gamma\varphi}^2 - t}. \tag{33}$$

For π exchange we use the parameters determined in a study of ω photoproduction [18]: $\Lambda_\pi = 0.7\,\text{GeV}$, $\Lambda^\pi_{\phi\gamma\pi} = 0.77\,\text{GeV}$. For the η exchange we choose $\Lambda_\eta = 1\,\text{GeV}$, $\Lambda_{\phi\gamma\eta} = 0.9\,\text{GeV}$. These parameters are close to that of the σ exchange introduced in Ref. [18] to fit the ρ photoproduction. This is reasonable since the mass of the considered σ meson is 500 MeV which is close to the mass of η meson.

Note that we do not consider the contribution of η' exchange. It is suppressed in PSE amplitude relative to the η exchange by a factor 5–6 because of the heavier mass of the propagator in Eq. (24) and the smaller value of $g_{\eta' NN}$, predicted by the SU(3) symmetry: $g_{\eta' NN} \simeq 0.49 g_{\eta NN}$ for the η-η' mixing angle around $-10°$ [36].

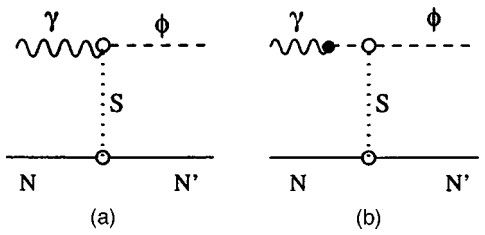

FIG. 4. Diagrammatic representations of (a) the scalar meson exchange in ϕ photoproduction and (b) VDM model for the scalar exchange.

C. Scalar meson exchange

The ϕ decay data suggest that the ϕ photoproduction amplitude could have contributions from the exchange of scalar mesons $a_0(980)$ with $I^G(J^{PC}) = 1^+(0^{++})$ and $f_0(980)$ and $\sigma = f_0(500)$ with $I^G(J^{PC}) = 0^+(0^{++})$. This is illustrated in Fig. 4. The $g_{\phi\gamma S}$ couplings are deeply related to the internal structure of the scalar mesons which is not well established and is still a subject of debate [38]. They are identified with conventional $q\bar{q}$ mesons [39,40], $q^2\bar{q}^2$ states [41,42], $K\bar{K}$ molecules [43,44], glueballs, and (or) hybrids [45]. Pennington and Morgan [46] have performed a precision fit to the available experimental data for scalar-isoscalar sector trying to understand the underground structure of this mesons. On the other hand, in a series of papers by Oller *et al.* [47] it is shown that the scalar mesons σ, f_0, a_0, κ appear naturally in the chiral unitary theory as a members of SU(3) nonet and their properties are in fair agreements with the data. For our estimation we make two assumptions: (i) the scalars σ, f_0, a_0, κ are members of unitary SU(3) nonet with (ii) $(q\bar{q})$-type internal structure. We also use SU(3) symmetry to fix the NNS coupling constants. In Appendix C we show how these can be determined from $g_{\rho\gamma\sigma}$ and $g_{NN\sigma}$ which are determined in a study [18] of ρ photoproduction.

The scalar-exchange amplitude is calculated from the following effective Lagrangians:

$$\mathcal{L}^{\text{int}}_{SNN} = g_{SNN}\bar{N}NS \tag{34}$$

and

$$\mathcal{L}^{\text{int}}_{\phi\gamma S} = \frac{e g_{\phi\gamma S}}{M_\phi}[\partial^\alpha\phi^\beta\partial_\alpha A_\beta - \partial^\alpha\phi^\beta\partial_\beta A_\alpha]S. \tag{35}$$

The above Lagrangians lead to the following expression for SE amplitude:

$$T_{fi} = -\sum_S \frac{e\, g_{\phi\gamma S} g_{SNN}}{t - M_S^2}[\bar{u}_{m_f}(p')u_{m_i}(p)]\varepsilon^*_{\phi\mu}\Gamma^{S\mu\nu}\varepsilon_{\gamma\nu}, \tag{36}$$

where

$$\Gamma^{S\mu\nu} = -\frac{(k\cdot q)g^{\mu\nu} - k^\mu q^\nu}{M_\phi}. \tag{37}$$

We note that the above expression can also be derived using current-field identity and VDM.

The $g_{\phi\gamma S}$ coupling constant is related to the width of radiative $\phi\to\gamma S$ decay

$$\Gamma(\phi\to\gamma S)=\frac{\alpha}{24}\,\frac{(M_\phi^2-M_S^2)^3}{M_\phi^5}g_{\phi\gamma S}^2. \tag{38}$$

The present accuracy [36] allows us to evaluate its upper limit:

$$\Gamma(\phi\to\gamma\pi^0\pi^0)<4.43\times10^{-6}\to|g_{\phi\gamma\sigma}|<\sqrt{3}\times0.18\simeq0.31,$$

$$\Gamma(\phi\to\gamma f_0)<4.43\times10^{-7}\to|g_{\phi\gamma f_0}|<1.77,$$

$$\Gamma(\phi\to\gamma a_0)<2.22\times10^{-5}\to|g_{\phi\gamma a_0}|<14, \tag{39}$$

where in the first case we assume that $\phi\to\gamma\pi^0\pi^0$ decay is dominated by σ and take $m_\sigma\simeq500$ MeV. One can see that the upper limit of $g_{\phi\gamma S}$'s has the same order of magnitude (and greater) as the couplings in $\phi\to\gamma\pi^0,\eta$ decays. So, the SE should be considered in more detail. With the large experimental uncertainties, we obviously need some theoretical input to fix the coupling constants. Our choice is detailed in Appendix C.

It is interesting to note here that the SE amplitude and the P_2 amplitude have the same spin dependence. The principal difference between them is in their phases. The SE amplitude is purely real, while P_2 is complex. We therefore expect that they can be distinguished clearly in polarization observables.

D. Direct ϕ meson radiation

This amplitude is shown in Fig. 1(c). The ϕNN and γNN interaction Lagrangians in obvious standard notations are

$$\mathcal{L}_{\phi NN}=-g_{\phi NN}\left(\bar{N}\gamma_\mu N\phi^\mu-\frac{\kappa_\phi}{2M_N}\bar{N}\sigma^{\mu\nu}N\partial_\nu\phi_\mu\right), \tag{40}$$

$$\mathcal{L}_{\gamma NN}=-e\left(\bar{N}\gamma_\mu NA^\mu-\frac{\kappa_N}{2M_N}\bar{N}\sigma^{\mu\nu}N\partial_\nu A_\mu\right), \tag{41}$$

with $\kappa_{p(n)}=1.79(-1.91)$. The resulting amplitude is

$$T_{fi}^{\rm C}=\bar{u}_{m_f}(p')M_{\mu\nu}^{\rm C}\varepsilon^{*\mu}_{\lambda_\phi}\varepsilon^{\nu}_{\lambda_\gamma}u_{m_i}(p), \tag{42}$$

$$M_{\mu\nu}^{\rm C}=eg_{\phi NN}\left[\Gamma_\mu^\phi(q)\frac{\not p_s+M_N}{p_s^2-M_N^2}\Gamma_\nu^\gamma(k)+\Gamma_\nu^\gamma(k)\frac{\not p_u+M_N}{p_u^2-M_N^2}\Gamma_\mu^\phi(q)\right], \tag{43}$$

where

$$\Gamma_\mu^\phi(q)=\gamma_\mu-i\frac{\kappa_\phi}{2M_N}\sigma_{\mu\nu}q^\nu,$$

$$\Gamma_\mu^\gamma(k)=f_N\gamma_\mu+i\frac{\kappa_N}{2M_N}\sigma_{\mu\nu}k^\nu, \tag{44}$$

and $f_{p(n)}=1(0)$ and $p_s=p+k$, $p_u=p-q$. The tensor parts for γ and ϕ in Eq. (44) have different signs, which reflect the difference between the incoming and outgoing particles.

The ϕ-radiation amplitude has a more complicated spin dependence than the PSE and SE amplitudes. For example, at $\theta=0$ the spin-flip transitions $\lambda_\gamma=\pm1\to\lambda_\phi=0$ along with $\lambda_i=\mp\frac{1}{2}\to\lambda_f=\pm\frac{1}{2}$ are allowed in ϕ radiation, but is forbidden in PSE and SE amplitudes. The ϕ-radiation amplitude is pure real and its sign is controlled by the constants of $g_{\phi NN},\kappa_\phi$. Following the theoretical estimation of Ref. [16] we choose $g_{\phi NN}=-0.24$ ($g_{\phi NN}^2/4\pi\simeq4.6\times10^{-3}$), $\kappa_\phi=0.2$, which are in qualitative agreement with the SU(3)-symmetry prediction.

Note, that in principle, the coupling ϕNN may be dressed by the cutoff form factor for off-shell nucleons. But this results in strong gauge invariance violation with respect to photon and ϕ meson fields alike [49,50]. To avoid this problem we use the prescription of Ref. [51], which favors for constant F^ϕ factors $F_s^\phi=F_u^\phi=1$. Thus, our prediction for ϕ radiation may be considered as an upper limit.

IV. DETERMINATION OF POMERON PARAMETERS

In the previous section, we have defined the parameters for the meson-exchange [Fig. 1(b)] and ϕ-radiation [Fig. 1(c)] amplitudes. These parameters have some uncertainties due to the errors of the data used in the determinations. For definiteness, we will present results using their mean values to evaluate the (π,η)-exchange and ϕ-radiation terms. For the scalar meson exchange, we will use their values determined by using the upper bound of the experimental values, as given in Eq. (39). We will discuss later how our results will be modified if the errors of these parameters are considered in our investigation.

We first observe that the meson-exchange and ϕ-radiation amplitudes only have appreciable contributions in the low energy region $\sqrt{s}<$ about 5 GeV. Because of a negative intercept $\alpha(0)=-0.75$, the contribution from the second Pomeron P_2 also drops very fast as energy increases. Consequently, the parameters of the first Pomeron P_1 can be fixed by fitting the cross sections in the high energy region. We find that the data of $d\sigma/dt(\theta=0)$ up to $\sqrt{s}\sim100$ GeV can be reproduced by choosing $C_1\sim2.-2.3$ and $s_1\sim1.5-2$ GeV^2. The uncertainties are due to the quality of the data. In considering the data in the low energy region, we therefore still have some freedom in adjusting the parameters of P_1.

To explore the roles of the second Pomeron P_2 and scalar meson exchange, we now turn to developing three models from fitting the data of ϕ photoproduction. Because of the insufficient accuracy of the available data, it is not advantageous to determine the parameters of each model by preforming a χ^2 fit. Instead, we simply demand that the total cross sections generated from each model must be consistent with the data within errors, and the greatest differences between them do not exceed 15% in the low energy region $W<5$ GeV. This is of course not very satisfactory, and must be improved to perform a χ^2 fit when more extensive and

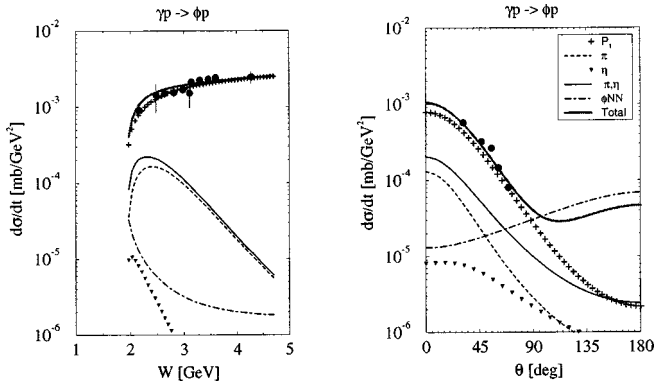

FIG. 5. The differential cross section $d\sigma/dt$ of $\gamma p \to \phi p$ reaction at $t=t_{\max}$ $(\theta=0)$ for model A as a function of the total energy $W=\sqrt{s}$ in the left panel. Data are taken from Refs. [52–54]. In the right panel we show the angular distribution at $E_\gamma=2$ GeV ($W=2.15$ GeV). Data are taken from Ref. [52].

precise data from new facilities become available in the near future. Nevertheless, the results obtained from using this naive *visual* fit should be sufficient for our present exploratory purposes.

Model A. In this model we consider only P_1, pseudoscalar meson (π,η) exchange amplitudes and the direct ϕ radiation. The model has three parameters C_1, s_1, and the slope B. The first two are fixed by fitting the energy dependence [52–54] of $d\sigma/dt$ at $t=t_{\max}(\theta=0)$: $C_1=2.09$, $s_1=1.6\,\mathrm{GeV}^2$. The slope $B_1=1.7\,\mathrm{GeV}^{-2}$ is found by fitting the data of angular distribution of $d\sigma/dt$ at $E_\gamma=2$ GeV [52].

Model B. This model is obtained by extending model A to include the P_2 amplitude. The slope parameter B_2 is chosen to be the same as B_1 of P_1 in order to maintain the same fit to the differential cross section $d\sigma/dt$ at $E_\gamma=2$ GeV. The model then has two additional parameters s_2 and C_2 for specifying the strength of the P_2 amplitude. In fact, they are not independent: decreasing s_2 leads to some increase of $|C_2|$, therefore for simplicity, we choose $s_2=0$. Because P_1 and P_2 amplitudes have different energy dependence, the energy dependence of $d\sigma/dt$ in the low energy region is sensitive to the ratio $\xi=C_2/C_1$. The parameter s_1 obviously also controls the energy dependence in the low energy region. For simplicity, we assume that the threshold behavior of P_1-Pomeron amplitude is defined by the natural scale $\sqrt{s_1}=M_N+M_\phi$. The model then only has two parameters C_1 and ξ. We find that the data can be fitted by setting $\xi=-0.55, C_1=2.34$. We find that this value of the ratio ξ is perhaps the maximum amount of the P_2 amplitude the data can accommodate. With a larger magnitude of ξ, the predicted energy dependence of the cross section has a shoulder-type behavior at $W\sim 2.5-3$ GeV, which might be in contradiction with the available data.

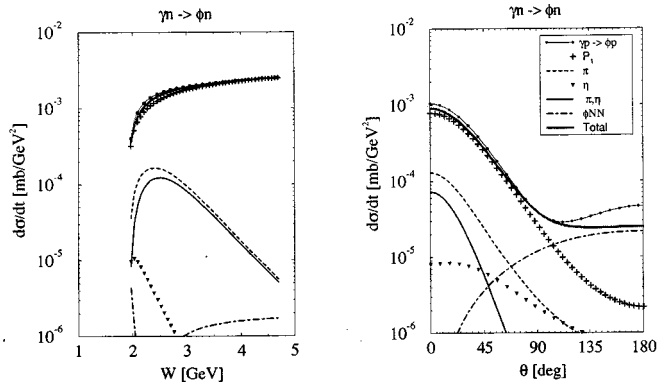

FIG. 6. The differential cross section of $\gamma n \to \phi n$ reaction for model A. Notations are the same as in Fig. 5. Dot-marked thin lines correspond to the $\gamma p \to \phi p$ reaction for the same model.

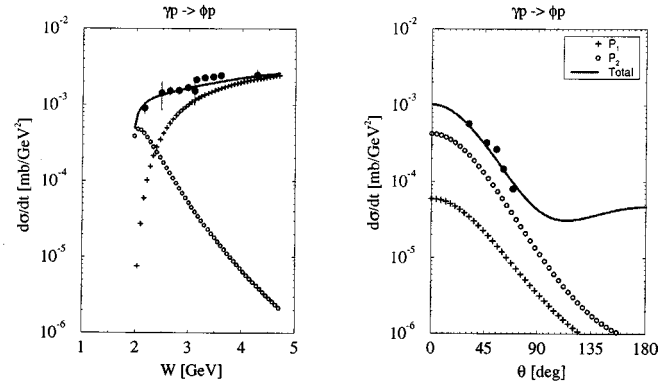

FIG. 7. The differential cross sections of $\gamma p \to \phi p$ reaction for model B. Notations are the same as in Fig. 5.

Model C. This model is obtained by extending model A to include scalar meson exchange amplitude. With the parameters given in Appendix C, we find that this additional amplitude has very small effect on the unpolarized cross sections. The data can be fitted by slightly modifying the P_1 parameters to $C_1=2.12, s_1=1.5\,\mathrm{GeV}^2$.

Let us first discuss the results from model A. In Fig. 5 we see that both the energy dependence (left panel) and angular distribution (right panel) of the unpolarized differential cross sections for the proton target can be described (thick solid curves) well. We also show the contributions from each mechanism. Obviously, the Pomeron exchange has the largest contribution. By comparing the solid curve (π,η) and the dashed curve (π), we see that the π exchange and η exchange interferes constructively. On the other hand, we see in Fig. 6 that they interfere destructively for the cross sec-

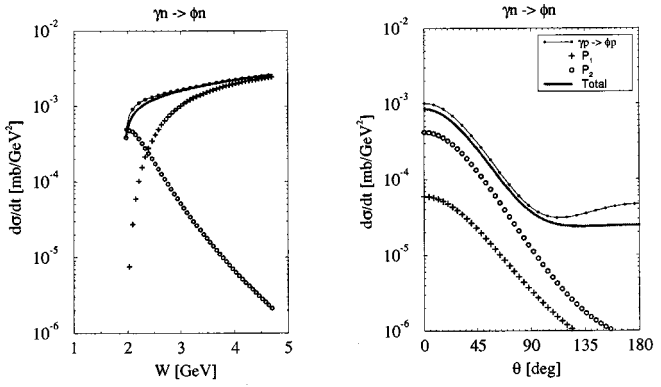

FIG. 8. The differential cross sections of $\gamma n \to \phi n$ reaction for model B. Notations are the same as in Fig. 6.

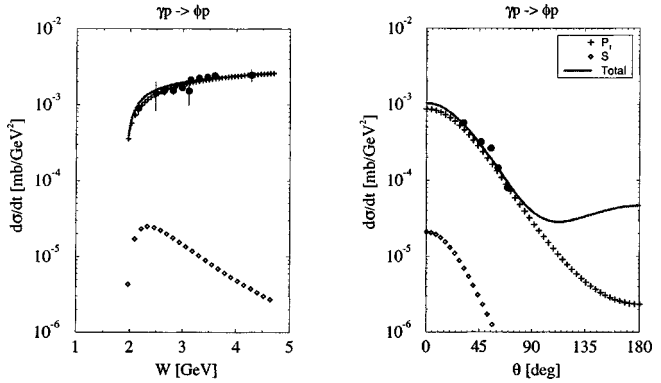

FIG. 9. The differential cross sections of $\gamma p \to \phi p$ reaction for model C. Notations are the same as in Fig. 5.

tions on the neutron target. In Fig. 6, we also show the results for the proton target. As discussed in Sec. III, this is due to the different sign of $g_{\pi^0 nn} = -g_{\pi^0 pp}$ while $g_{\eta pp} = g_{\eta nn}$. Clearly, this isotopic effect cannot be tested by examining the unpolarized cross sections. It is also interesting to note that the ϕ-radiation contribution (dot-dashed curves) dominate the cross sections at large angles. However, its magnitudes are perhaps too small to be observed experimentally.

The results for model B are displayed in Figs. 7 and 8. We see that the contributions from P_1 and P_2 have very different energy dependence. This is due to the difference in the their intercepts: $\alpha_1(0) = 1.08, \alpha_2(0) = -0.75$. The full calculation (thick solid curves) contain contributions from (π, η) exchange and the ϕ-radiation mechanism. The isotopic effect shown in Fig. 8 is also too small for experimental tests.

In Figs. 9 and 10, we see that the data can also described equally well by model C. We also show the individual contributions from P_1 and scalar meson $(\sigma + a_0 + f_0)$ exchange. The full calculations (thick solid curves) include the contributions from (π, η) exchange and ϕ radiation. Obviously, the scalar meson exchange has negligible effects on the unpolarized cross section. Again the isotopic effects shown in Fig. 10 are too small for experimental tests.

In Fig. 11 we show the differential cross section of $\gamma p \to \phi p$ reaction at $E_\gamma = 3.25$ GeV for models A and B. One can see that the models describe the data with approximately

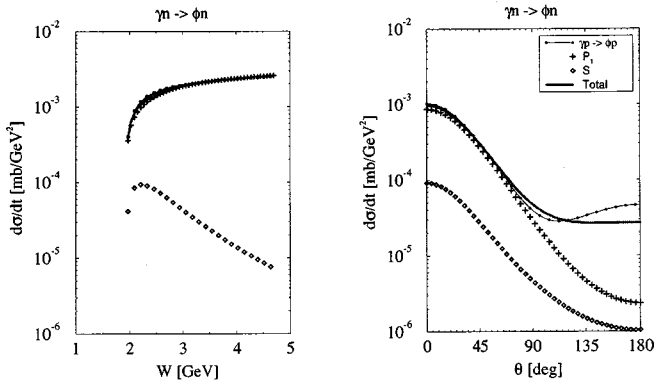

FIG. 10. The differential cross sections of $\gamma n \to \phi n$ reaction for model C. Notations are the same as in Fig. 6.

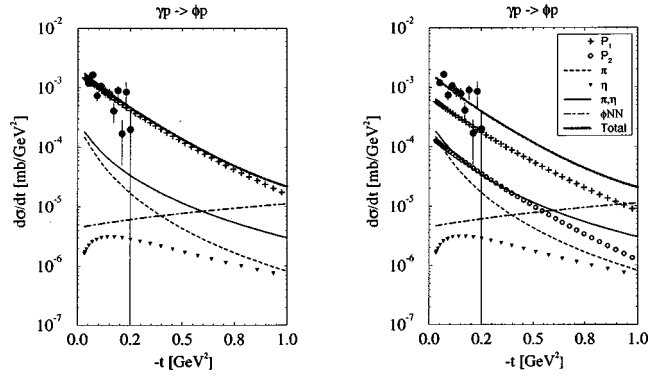

FIG. 11. The differential cross sections of $\gamma p \to \phi p$ reaction at $E_\gamma = 3.25$ GeV $(W = 2.64$ GeV) for model A (left panel) and B (right panel). Data are taken from Ref. [54].

equal quality and at the present level of the data accuracy it is difficult to give preference to one of them. We now turn to the investigation of whether other observables can be used to distinguish these three models and isotopic effects.

V. PREDICTIONS OF THE DENSITY MATRIX ELEMENTS FOR ϕ MESON

In Appendix A, we have given formula for calculating the K^+K^- angular distributions in terms of density matrix elements $\rho^{\alpha}_{\lambda',\lambda}$ of ϕ meson. The angular distributions (A19) due to unpolarized incident photons are only determined by ρ^0. For circularly (linearly) polarized incident photons, the angular distributions (20) [Eq. (21)] are calculated from ρ^0 and ρ^3 (ρ^0, ρ^1, and ρ^2). It is therefore sufficient to only present our predictions of these density matrix elements defined in the GJ system. We will show the dependence of these matrix elements on the angle θ of the outgoing ϕ in c.m.s. The left (right) panels of Figs. 11–24 show the results for $\gamma p \to \phi p$ $(\gamma n \to \phi n)$ at $E_\gamma = 2$ GeV. Our main interest is to examine how the predicted density matrices depend on the models which are constructed in the previous section to give an equally good description of the available data of unpolarized differential cross sections $d\sigma/dt$. We will also investigate the energy dependence of ϕ decay asymmetry and its dependence on the ηNN and ϕNN coupling constants.

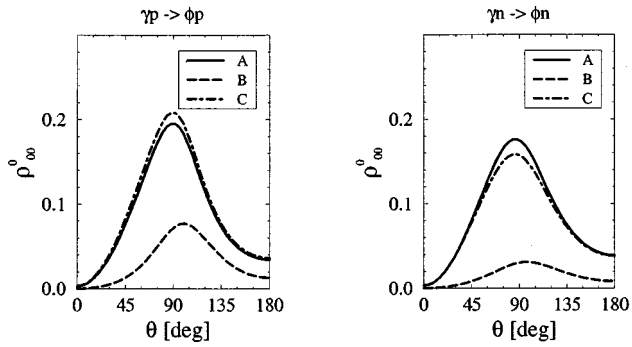

FIG. 12. Spin-density matrix element ρ^0_{00} for the different models. Left and right panels correspond to $\gamma p \to p\phi$ and $\gamma n \to n\phi$ reactions, respectively.

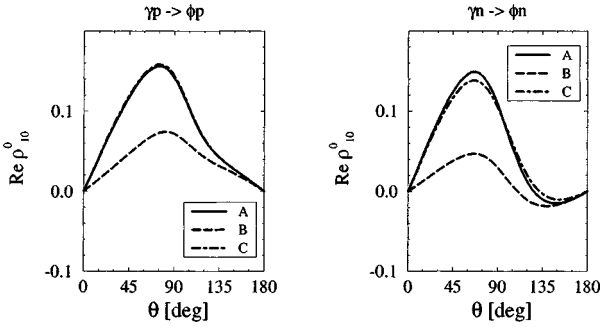

FIG. 13. Spin-density matrix element $\mathrm{Re}\,\rho^0_{10}$ for the different models. Notations are the same as in Fig. 12.

The matrix elements ρ^0_{00}, $\mathrm{Re}\,\rho^0_{10}$, and $\mathrm{Re}\,\rho^0_{1-1}$, which determine the K^+K^- angular distributions with unpolarized incident photons, are shown in Figs. 12–14. As seen in Eqs. (A17) and (A19), the matrix element ρ^0_{00} is responsible for the azimuthal angle-averaged unpolarized decay distribution $\overline{\mathcal{W}}$ defined in Eq. (A22)

$$\overline{\mathcal{W}}^{\,0}=\frac{3}{4\pi}\left[\frac{1}{2}(1-\rho^0_{00})+\frac{1}{2}(3\rho^0_{00}-1)\cos^2\Theta\right].$$

We see from Figs. 12 and 13 that the predictions from models A and C are very similar. However, model B, which includes the second Pomeron P_2, yields a much smaller ρ^0_{00}. At $\theta\sim 90°$ where ρ^0_{00} has the maximum value, we obtain

$$\overline{\mathcal{W}}^{\,0}\simeq\frac{3}{8\pi}(0.36+0.43\sin^2\Theta), \tag{45}$$

for models A and C, and

$$\overline{\mathcal{W}}^{\,0}\simeq\frac{3}{8\pi}(0.14+0.79\sin^2\Theta) \tag{46}$$

for model B. Obviously, model B can be clearly distinguished from the other two models from a measurement of this Θ distribution of the emitted K^+K^- pair. This, of course, will be a good test of the conjectured P_2 Pomeron. Here we note that the above two expressions are very different from the predicted from using helicity conserving amplitudes (HCM) (see Appendix A)

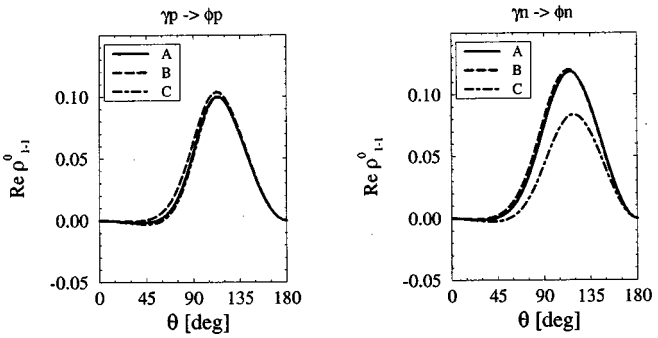

FIG. 14. Spin-density matrix element $\mathrm{Re}\,\rho^0_{1-1}$ for the different models. Notations are the same as in Fig. 12.

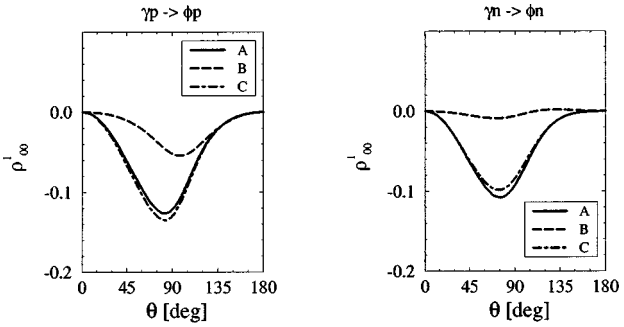

FIG. 15. Spin-density matrix element ρ^1_{00} for the different models. Notations are the same as in Fig. 12.

$$\overline{\mathcal{W}}^{\,0}_{0}\simeq\frac{3}{8\pi}\sin^2\Theta. \tag{47}$$

As discussed in Appendix A, HCM is due to either a pure natural parity exchange (scalar exchange) or a pure unnatural parity exchange (pseudoscalar meson exchange) mechanisms. The difference between Eqs. (45), (46) and Eq. (47) therefore measure the deviation of the constructed models from the helicity conserving mechanisms. This deviation of course is due to the interference between different amplitudes illustrated in Fig. 1.

From Eq. (A17), we see that $\mathrm{Re}\,\rho^0_{10}$, and $\mathrm{Re}\,\rho^0_{1-1}$, shown in Figs. 13 and 14, determine the azimuthal angle dependence of $\mathcal{W}^0(\cos\Theta,\Phi)$. The measurements of Φ dependence obviously will provide further test of the considered models. Here we see again that the predictions from models A and C are in general very similar. The large differences between the dashed curves and the other two curves suggest that a measurement of Φ dependence can be very useful to distinguish model B from the other two models.

In Figs. 15–18 we show our result for ρ^1 matrix. As seen in Eqs. (A17) and (A21), this density matrix is responsible for the K^+K^- distributions from ϕ photoproduction reactions with incident linear polarized photons. For example, the distributions averaged over the azimuthal angle Φ are only determined by the matrix elements ρ^1_{00} and ρ^1_{11}

$$\overline{\mathcal{W}}^{\,1}(\cos\Theta)=\frac{3}{4\pi}[\rho^1_{11}+(\rho^1_{00}-\rho^1_{11})\cos^2\Theta]. \tag{48}$$

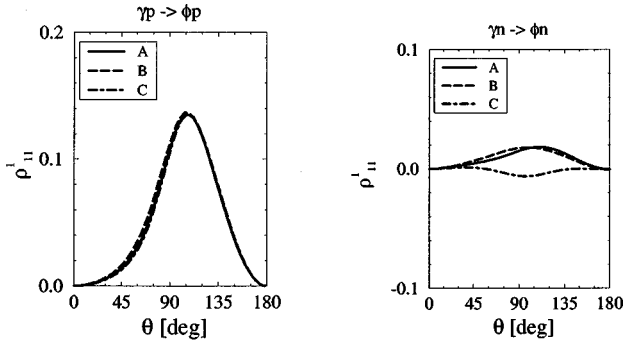

FIG. 16. Spin-density matrix element ρ^1_{11} for the different models. Notations are the same as in Fig. 12.

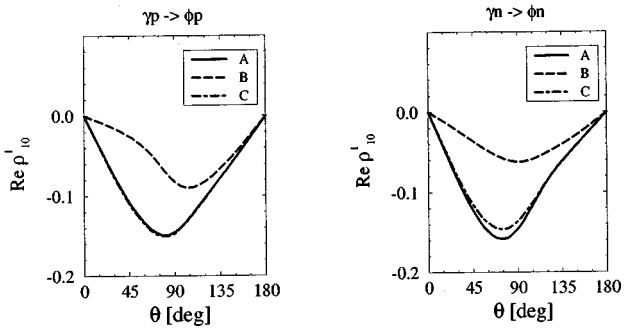

FIG. 17. Spin-density matrix element $\mathrm{Re}\,\rho^1_{10}$ for the different models. Notations are the same as in Fig. 12.

The above expression suggests that $\overline{W}(\cos\Theta)$ can also be used to distinguish model B from the other two models since its ρ^1_{00} in Fig. 15 is much smaller.

The most interesting is the antidiagonal $\mathrm{Re}\,\rho^1_{1-1}$. As shown in Appendix A, the helicity conserving mechanisms predict $\rho^1_{1-1}=\pm\frac{1}{2}$ for either a natural or a unnatural parity exchanges. In Fig. 18, we see that all considered models predict a strong violation of this prediction of helicity conserving mechanism. This of course is due to the interference between different mechanisms shown in Fig. 1. We find that the relatively large contribution of the direct ϕ radiation, which is a mixture of natural and unnatural parity exchange, leads to decreasing of $\mathrm{Re}\,\rho^1_{1-1}$ at large θ. That is also seen in the θ dependence of Σ_ϕ and P_σ, shown in Figs. 19, 20. Both quantities are controlled by ρ^1_{1-1} [cf. Eqs. (A30), (A37)] and the both differ significantly from the helicity conserving mechanism prediction $\Sigma_\phi=P_\sigma=2\rho^1_{1-1}=\pm 1$.

Figures 21, 22 show the matrix elements of matrix ρ^2. We see from Eq. (A21) that this quantity together with ρ^1 matrix are responsible for the angular distribution in reactions with arbitrary linearly polarized photons. The most interesting here is $\mathrm{Im}\,\rho^2_{1-1}$ matrix element, which plays the same role as ρ^1_{1-1} in the above discussion.

Figures 23, 24 show $\mathrm{Im}\,\rho^3_{10}$ and $\mathrm{Im}\,\rho^3_{1-1}$, which determine, via Eq. (A20), the angular distribution in reactions with the circularly polarized beam. HCM predicts zero values for them and, as a consequence, zero asymmetry between cross sections with positive and negative beam polarization. The finite value of $\mathrm{Im}\,\rho^3_{1-1}$ and $\mathrm{Im}\,\rho^3_{10}$ leads, respectively, to the finite asymmetry.

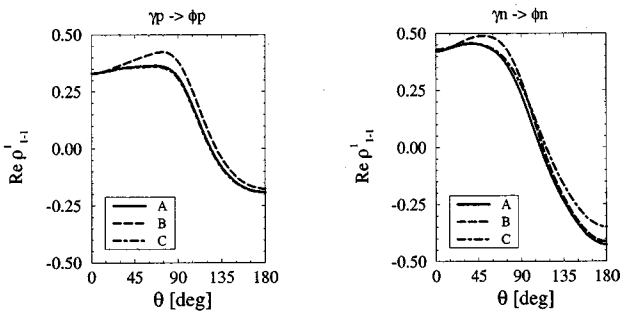

FIG. 18. Spin-density matrix element $\mathrm{Re}\,\rho^1_{1-1}$ for the different models. Notations are the same as in Fig. 12.

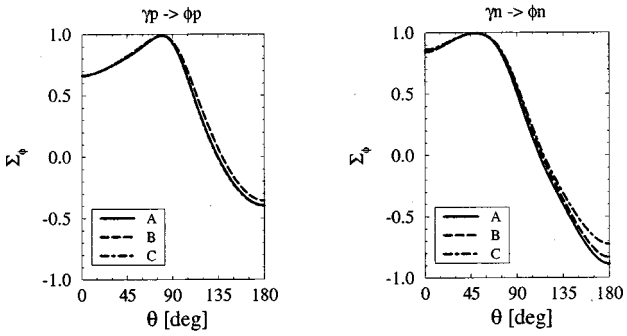

FIG. 19. The ϕ decay asymmetry Σ_ϕ for the different models. Notations are the same as in Fig. 12.

Figure 25 shows the dependence of the ϕ decay asymmetry Σ_ϕ as function of the photon energy at $\theta=0$ for $\gamma p,n$ reactions for model B. One can see a strong deviation from the HCM prediction $\Sigma_\phi=1$ and a clear difference between predictions for γp and γn reactions at $E_\gamma\simeq 2-4$ GeV.

The close inspection of the spin-density matrix elements shows that some of them are very sensitive to the Pomeron structure of the diffractive amplitudes. They are ρ^0_{00}, $\mathrm{Re}\,\rho^0_{10}$, ρ^1_{00}, $\mathrm{Re}\,\rho^1_{10}$, $\mathrm{Im}\,\rho^2_{10}$, $\mathrm{Im}\,\rho^3_{10}$, $\mathrm{Im}\,\rho^3_{1-1}$. These matrix elements and the corresponding K^+K^- angular distributions may be used for understanding the role of P_2 amplitudes at low energy.

Coming back to the isotopic effect in ϕ photoproduction we notice that at small θ the difference between γp and γn reactions is associated by the difference in π-η interference in PSE amplitude and it increases with increase the ηNN coupling constant. This effect is shown in Fig. 26 (left panel) where we display dependence of Σ_ϕ on $g_{\eta NN}$ at $E_\gamma=2$ GeV and $\theta=0$ for the model B. In this calculation increasing (decreasing) $g_{\eta NN}$ is attended with decrease (increase) of the strength ξ of the P_2 amplitude. At large θ, Σ_ϕ is controlled by the direct ϕ radiation. Figure 26 (right panel) shows dependence of Σ_ϕ on $g_{\phi NN}$ at $E_\gamma=2$ GeV and $\theta=135°$ for model B. One can see some decreasing of Σ_ϕ with $g^2_{\phi NN}/4\pi$. The other models predict the same behavior of Σ_ϕ. So, the ϕ photoproduction may give independent information about the dynamics of the ηNN and ϕNN interactions.

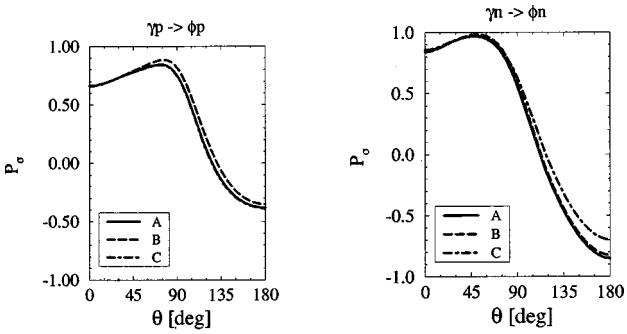

FIG. 20. The ϕ decay asymmetry P_σ for the different models. Notations are the same as in Fig. 12.

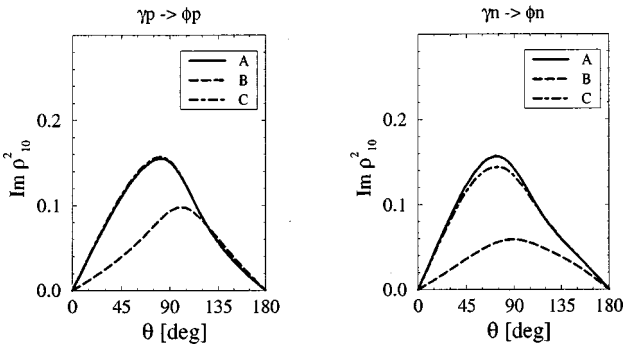

FIG. 21. Spin-density matrix element $\mathrm{Im}\,\rho^2_{10}$ for the different models. Notations are the same as in Fig. 12.

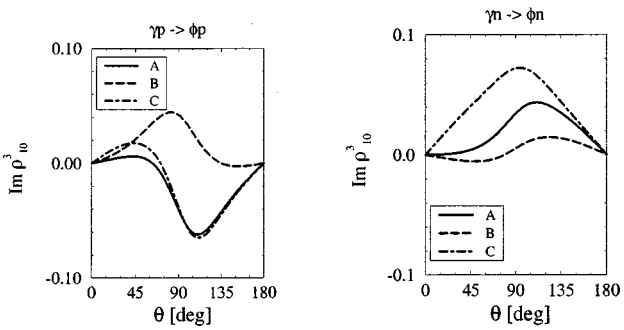

FIG. 23. Spin-density matrix element $\mathrm{Im}\,\rho^3_{10}$ for the different models. Notations are the same as in Fig. 12.

We note here that the isotopic effects illustrated in Figs. 25 and 26 are obtained by using the mean values of the photon-meson coupling constants $|g_{\phi\gamma\pi}|=0.141\pm0.007$ and $|g_{\phi\gamma\eta}|=0.707\pm0.017$. As discussed in Sec. III, the uncertainties of these two parameters are due to the data used in our determinations, as seen in Eq. (32). We find that the uncertainties of these two parameters only give an about 4 and 11% change of the PSE amplitude in the γp, γn reactions, respectively, for the kinematics considered here. Note that this amplitude is much smaller than the Pomeron exchange amplitudes (see Fig. 5). Consequently, its uncertainty does not significantly change all of the models we have constructed. For example, the parameter $\xi=C_2/C_1$ of model B has about 5% uncertainty. This also leads to an uncertainty in the predicted isotopic effect at 2 GeV: $\Sigma_\phi(\gamma n)-\Sigma_\phi(\gamma p)=0.18\pm0.02$. This gives some measure about the accuracy needed for designing future experiments to verify the predicted isotopic effects illustrated in Figs. 25 and 26.

VI. OTHER DOUBLE POLARIZATION OBSERVABLES

In the previous section we have considered double polarization connected with the boson sector of the process, namely, with the photon polarization and ϕ-meson helicity (or K^+K^- angular distribution). In some cases we found definite difference between prediction of the ''realistic models'' and HCM, and the difference between different models.

The difference between different models may be seen also in double polarization observables which operate with boson (photon or ϕ) and fermion (initial or recoil nucleon). Here we discuss two of them: beam target C_{zz}^{BT} and beam recoil $C_{zx'}^{\mathrm{BR}}$ asymmetries [see Eqs. (10), (11)]. These asymmetries as a function of the ϕ-production angle at $E_\gamma=2$ GeV are shown in Figs. 27,28.

The beam target C_{zz}^{BT} asymmetry is proportional to the product of the natural and unnatural parity exchange amplitudes $\mathrm{Re}(T^{\mathrm{N}}\cdot T^{\mathrm{U}*})$. In our case at small θ for models A, B it is a product of the small real part of the $P_{1,2}$ and pseudoscalar exchange and the natural parity exchange part of direct ϕ-radiation amplitudes. Say, for the almost pure imaginary P_1 amplitude, $C_{zz}^{\mathrm{BT}}(\theta=0)\simeq0$ for model A [21]. For model C it is proportional to the product of the scalar and pseudoscalar exchange amplitudes. In each model there is definite contribution of the ϕ direct radiation. The thin short dashed lines correspond to calculation with $g_{\phi NN}=0$ in model B. One can see, that the contribution of direct ϕ radiation is more essential at large θ and changes the asymmetries qualitatively.

In some sense similar consideration holds for $C_{zx'}^{\mathrm{BR}}$ asymmetry in Fig. 28, but here the interference term is proportional to product of fermion spin conserving and spin-flip amplitudes. The latter vanishes at $\theta=0,\pi$. Again one can see differences between different models and between γp and

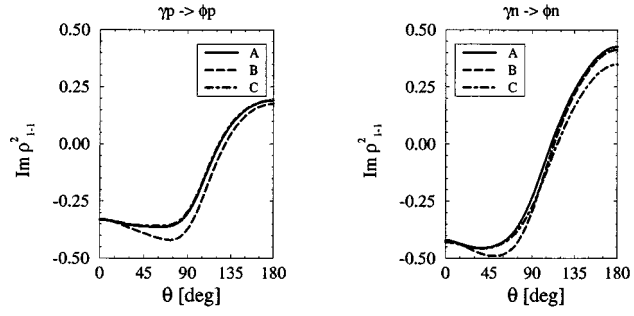

FIG. 22. Spin-density matrix element $\mathrm{Im}\,\rho^2_{1-1}$ for the different models. Notations are the same as in Fig. 12.

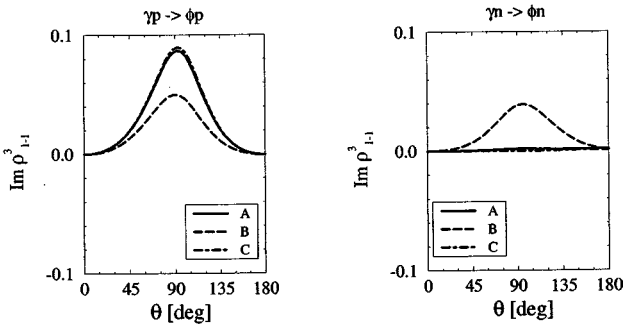

FIG. 24. Spin-density matrix element $\mathrm{Im}\,\rho^3_{1-1}$ for the different models. Notations are the same as in Fig. 12.

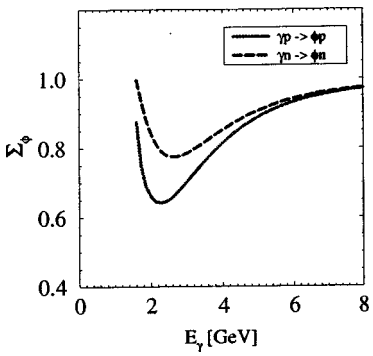

FIG. 25. The ϕ decay asymmetry Σ_ϕ at $\theta=0$ for model B as a function of the photon energy.

γn reactions. By this it is meant, that from the described double-polarization observables one can select from the different models.

VII. SUMMARY

We have analyzed the ϕ photoproduction amplitude in the $\sqrt{s}\sim 2-5$ GeV region based on the Pomeron-exchange and meson-exchange mechanisms. The parameters that are needed to evaluate the pseudoscalar mesons (π,η) exchange, scalar mesons (σ,a_0,f_0) exchange, and the ϕ radiation from the nucleon are determined from SU(3) symmetry and ϕ decay widths. In addition to the well established Pomeron exchange with an intercept $\alpha(0)\sim 1.08$, we have investigated the role of a second Pomeron with $\alpha(0)<0$, as inspired by the glueball $(J^\pi=0^+, M_b^2\sim 3\ \mathrm{GeV}^2)$ predicted by the lattice QCD calculation and dual Ginsburg-Landau model.

To explore the relative importance between the second Pomeron and scalar meson exchange, we have constructed three models which can give equally good fits to the existing very limited data. It is shown that the second Pomeron can be identified by investigating various spin observables associated with the $\phi\to K^+K^-$ decays in the γp and γn reactions with polarized photons.

We have found that the t dependence of cross sections are more promising for investigating meson-exchange and

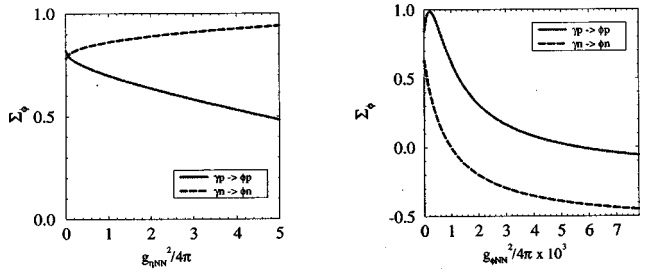

FIG. 26. The ϕ decay asymmetry Σ_ϕ for model B. Left panel: the dependence of Σ_ϕ on the ηNN coupling constant at $\theta=0$. Right panel: the dependence of Σ_ϕ on the ϕNN coupling constant at $\theta=135°$.

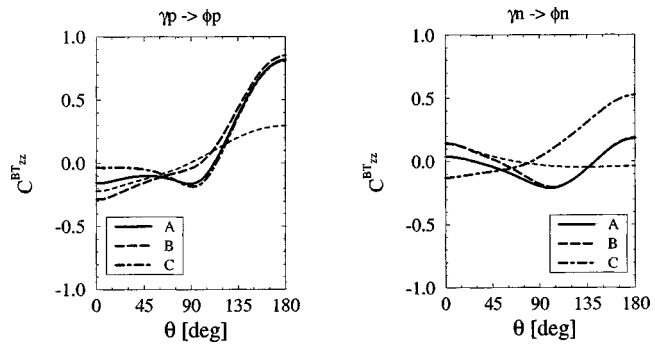

FIG. 27. Double beam target asymmetry C_{zz}^{BT} for $\gamma p\to\phi p$ (left panel) and for $\gamma n\to\phi n$ (right panel) reactions in the three models. The thin dashed lines correspond to $g_{\phi NN}=0$ in model B.

ϕ-radiation mechanisms. The cross sections at large angles can be used to determine the ϕNN coupling constant. The target isotopic effect on the ϕ decay asymmetry Σ_ϕ is found to be sensitive to the interference between the π and η exchange amplitudes and hence can be used to study the ηNN coupling constant.

We have also found that the double polarization beam-target asymmetries are small at $\theta\to 0$ for all models considered. As demonstrated in Refs. [15,21], this implies that any significant beam-target asymmetry measured in future experiments will be the manifestation of the direct $s\bar{s}$ knockout from the nucleon.

Finally, we emphasize that the present investigation is very exploratory, owing to the lack of precise data at a few GeV. It is highly desirable to obtain more data from the new facilities such as LEPS of SPring-8 in Japan and TJNAF. The polarization observables will be most useful for future theoretical investigations.

ACKNOWLEDGMENTS

We gratefully acknowledge fruitful discussions with M. Fujiwara, H. Gao, T. Hotta, T. Morii, Y. Oh, and E. Oset. Especially, we wish to thank T. Nakano who initiated this

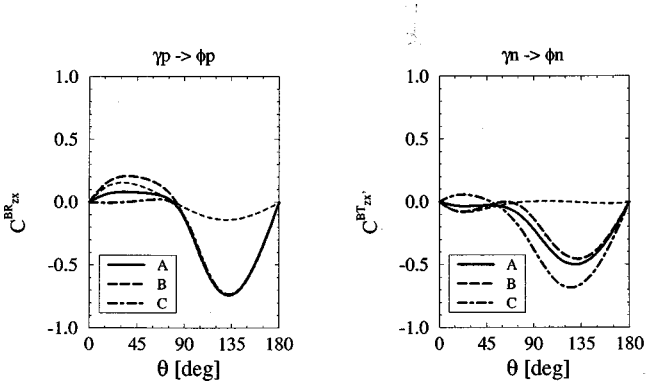

FIG. 28. Double beam recoil asymmetry $C_{zx'}^{\mathrm{BR}}$ for $\gamma p\to\phi p$ (left panel) and $\gamma n\to\phi n$ (right panel) reactions for the three models. Notations are the same as in Fig. 27.

study with first estimation of the P_2 exchange channel. A.I.T. appreciates the support of Monbusho, the warm hospitality of the Research Center for Nuclear Physics of Osaka University, and H. Ejiri for his encouragement. This work was also supported partially by the U.S. Department of Energy, Nuclear Physics Division, under Contract No. W-31-109-ENG-38.

APPENDIX A: GENERAL FORM OF ANGULAR DISTRIBUTION

In this appendix we give formula defined the ϕ decay angular distributions for the arbitrary polarized photon beam. Starting from Eq. (7) and noting that $\lambda_{ab}=\lambda_a-\lambda_b=0$ in $\phi\to K^+K^-$ $\lambda_{ab}=\lambda_a-\lambda_b=\pm 1$ in $\phi\to e^+e^-$, one obtains

$$\mathcal{W}^{K^+K^-}(\cos\Theta,\Phi)=\frac{3}{4\pi}\sum_{\lambda\lambda'} D^{1*}_{\lambda 0}(\Phi,\Theta,-\Phi)\rho_{\lambda\lambda'}D^{1}_{\lambda' 0}(\Phi,\Theta,-\Phi), \tag{A1}$$

$$\mathcal{W}^{e^+e^-}(\cos\Theta,\Phi)=\frac{3}{8\pi}\sum_{rr'} \{D^{1*}_{r1}(\Phi,\Theta,-\Phi)\rho_{\lambda\lambda'}D^{1}_{r' 1}(\Phi,\Theta,-\Phi)+D^{1*}_{\lambda -1}(\Phi,\Theta,-\Phi)\rho_{\lambda\lambda'}D^{1}_{\lambda' -1}(\Phi,\Theta,-\Phi)\}, \tag{A2}$$

where $\rho_{\lambda,\lambda'}$ is the density matrix defined in Eq. (8) and λ is the helicity of the ϕ meson. The relevant Wigner rotation functions are given by

$$D^1_{l0}(\Phi,\Theta,-\Phi)=\frac{-l}{\sqrt{2}}\sin\Theta e^{-il\Phi},$$

$$D^1_{0l}(\Phi,\Theta,-\Phi)=\frac{l}{\sqrt{2}}\sin\Theta e^{il\Phi},$$

$$D^1_{00}(\Phi,\Theta,-\Phi)=\cos\Theta,$$

$$D^1_{ll'}(\Phi,\Theta,-\Phi)=\frac{1}{2}(1+ll'\cos\Theta)e^{-i(l-l')\Phi}, \tag{A3}$$

for $l,l'=\pm 1$. Using the fact that $\rho_{rr'}$ is Hermitian , $\rho_{rr'}=\rho^*_{r'r}$, and the above the explicit forms of D functions, we get

$$\mathcal{W}^{K^+K^-}(\cos\Theta,\Phi)=\frac{3}{4\pi}\left(\frac{1}{2}(\rho_{11}+\rho_{-1-1})\sin^2\Theta+\rho_{00}\cos^2\Theta+\frac{1}{\sqrt{2}}(-\mathrm{Re}\,\rho_{10}+\mathrm{Re}\,\rho_{-10})\sin 2\Theta\cos\Phi\right.$$
$$\left.+\frac{1}{\sqrt{2}}(\mathrm{Im}\,\rho_{10}+\mathrm{Im}\,\rho_{-10})\sin 2\Theta\sin\Phi-\mathrm{Re}\,\rho_{1-1}\sin^2\Theta\cos 2\Phi+\mathrm{Im}\,\rho_{1-1}\sin^2\Theta\sin 2\Phi\right), \tag{A4}$$

$$\mathcal{W}^{e^+e^-}(\cos\Theta,\Phi)=\frac{3}{8\pi}\left(\frac{1}{2}(\rho_{11}+\rho_{-1-1})(1+\cos^2\Theta)+\rho_{00}\sin^2\Theta+\frac{1}{\sqrt{2}}(\mathrm{Re}\,\rho_{10}-\mathrm{Re}\,\rho_{-10})\sin 2\Theta\cos\Phi\right.$$
$$\left.-\frac{1}{\sqrt{2}}(\mathrm{Im}\,\rho_{10}+\mathrm{Im}\,\rho_{-10})\sin 2\Theta\sin\Phi+\mathrm{Re}\,\rho_{1-1}\sin^2\Theta\cos 2\Phi-\mathrm{Im}\,\rho_{1-1}\sin^2\Theta\sin 2\Phi\right). \tag{A5}$$

We see from Eqs. (A4) and (A5) that the decay distributions integrated over the azimuthal angle depend only on the diagonal matrix elements

$$\mathcal{W}^{K^+K^-}(\cos\Theta)=\frac{3}{4}(1-\rho_{00})(1+B^{K^+K^-}\cos^2\Theta),$$

$$\mathcal{W}^{e^+e^-}(\cos\Theta)=\frac{3}{8}(1+\rho_{00})(1+B^{e^+e^-}\cos^2\Theta), \tag{A6}$$

where we use the normalization condition $\rho_{11}+\rho_{-1-1}+\rho_{00}=1$ and introduce the ϕ decay anisotropy

$$B^{K^+K^-}=-(1-3\rho_{00})/(1-\rho_{00}),$$

$$B^{e^+e^-}=(1-3\rho_{00})/(1+\rho_{00}). \tag{A7}$$

1. Dependence of angular distributions of the K^+K^- pair on the photon polarizations

The photon density matrix can be written as

$$\rho(\gamma)=\frac{1}{2}(1+\mathbf{P}_\gamma\cdot\boldsymbol{\sigma}), \tag{A8}$$

where $\boldsymbol{\sigma}$ is the Pauli operator and $\boldsymbol{P}_\gamma$ specifies the photon polarization. Consequently, for circular polarization with $\lambda=\pm1$ we have

$$\mathbf{P}_\gamma=P_\gamma(0,0,\lambda_\gamma). \tag{A9}$$

The linearly polarized photon is defined by

$$\mathbf{P}_\gamma=P_\gamma(-\cos 2\psi,-\sin 2\psi,0), \tag{A10}$$

where ψ denotes the angle between the photon polarization vector and the ϕ-meson production plane (i.e., **XZ** plane). The photon polarization vector is accordingly defined as $\boldsymbol{\varepsilon}_\gamma=(\cos\psi,\sin\psi,0)$. In the above expressions, P_γ denotes the strength of the polarization $(0\leqslant P_\gamma\leqslant 1)$.

Now, using Eq. (A8) we can decompose the ϕ density matrix ρ, defined in Eq. (8), as

$$\rho=\rho^0+\sum_{\alpha=1}^{3}P_\gamma^\alpha\rho^\alpha, \tag{A11}$$

where

$$\rho^0=TT^\dagger,\quad \rho^\alpha=T\sigma^\alpha(\gamma)T^\dagger, \tag{A12}$$

with $\alpha=(1,2,3)$. In terms of helicity amplitudes $T_{\lambda_f\lambda;\lambda_i\lambda_\gamma}$, they can be written explicitly as

$$\rho^0_{\lambda\lambda'}=\frac{1}{N}\sum_{\lambda_\gamma,\lambda_i,\lambda_f}T_{\lambda_f\lambda;\lambda_i\lambda_\gamma}T^*_{\lambda_f\lambda';\lambda_i\lambda_\gamma},$$

$$\rho^1_{\lambda\lambda'}=\frac{1}{N}\sum_{\lambda_\gamma,\lambda_i,\lambda_f}T_{\lambda_f\lambda;\lambda_i-\lambda_\gamma}T^*_{\lambda_f\lambda';\lambda_i\lambda_\gamma},$$

$$\rho^2_{\lambda\lambda'}=\frac{i}{N}\sum_{\lambda_\gamma,\lambda_i,\lambda_f}\lambda_\gamma T_{\lambda_f\lambda;\lambda_i-\lambda_\gamma}T^*_{\lambda_f\lambda';\lambda_i\lambda_\gamma},$$

$$\rho^3_{\lambda\lambda'}=\frac{1}{N}\sum_{\lambda_\gamma,\lambda_i,\lambda_f}\lambda_\gamma T_{\lambda_f\lambda;\lambda_i\lambda_\gamma}T^*_{\lambda_f\lambda';\lambda_i\lambda_\gamma}. \tag{A13}$$

By using Eq. (A11), the normalized angular distribution (A4) can be decomposed into

$$\mathcal{W}(\cos\Theta,\Phi)=\mathcal{W}^0(\cos\Theta,\Phi)+\sum_{\alpha=1}^{3}P_\gamma^\alpha\mathcal{W}^\alpha(\cos\Theta,\Phi), \tag{A14}$$

where $\mathcal{W}^\alpha$ is of the same form of Eq. (7) except that $\rho_{\lambda,\lambda'}$ is replaced by $\rho^\alpha_{\lambda,\lambda'}$.

By using the symmetry property of the helicity amplitudes

$$T_{-\lambda_f-\lambda;-\lambda_i-\lambda_\gamma}=(-1)^{(\lambda-\lambda_f)-(\lambda_\gamma-\lambda_i)}T_{\lambda_f\lambda;\lambda_i\lambda_\gamma}, \tag{A15}$$

we have the following relations:

$$\rho^\alpha_{\lambda\lambda'}=(-1)^{\lambda-\lambda'}\rho^\alpha_{-\lambda-\lambda'}\quad\text{for }(\alpha=0,1),$$

$$\rho^\alpha_{\lambda\lambda'}=-(-1)^{\lambda-\lambda'}\rho^\alpha_{-\lambda-\lambda'}\quad\text{for }(\alpha=2,3). \tag{A16}$$

Equation (A16) means that ρ^0_{1-1} and ρ^1_{1-1} are real and ρ^2_{1-1} and ρ^3_{1-1} are purely imaginary. In addition, we have for $\alpha=0,1$ that $\rho^\alpha_{-1-1}=\rho^\alpha_{11}$, $\rho^\alpha_{-10}=-\rho^\alpha_{10}$ and $\mathrm{Tr}\,\rho^\alpha=1$. These relations greatly reduce the number of independent matrix elements.

For simplicity, we will focus on the $\phi\to K^+K^-$ decay. Generalization for $\phi\to e^+e^-$ decay is straightforward. By using the symmetry properties described above, we have for $\alpha=0,1$

$$W^0(\cos\Theta,\Phi)=\frac{3}{4\pi}\left\{\frac{1}{2}(1-\rho^0_{00})+\frac{1}{2}(3\rho^0_{00}-1)\cos^2\Theta-\sqrt{2}\,\mathrm{Re}\,\rho^0_{10}\sin 2\Theta\cos\Phi-\mathrm{Re}\,\rho^0_{1-1}\sin^2\Theta\cos 2\Phi\right\},$$

$$W^1(\cos\Theta,\Phi)=\frac{3}{4\pi}\{\rho^1_{11}\sin^2\Theta+\rho^1_{00}\cos^2\Theta-\sqrt{2}\,\mathrm{Re}\,\rho^1_{10}\sin 2\Theta\cos\Phi-\mathrm{Re}\,\rho^1_{1-1}\sin^2\Theta\cos 2\Phi\}. \tag{A17}$$

For $\alpha=2,3$ we also have the symmetry properties that $\rho^\alpha_{-1-1}=-\rho^\alpha_{11}$, $\rho^\alpha_{-10}=\rho^\alpha_{10}$, and $\rho^\alpha_{00}=0$. As a consequence, we find

$$\mathcal{W}^2(\cos\Theta,\Phi)=\frac{3}{4\pi}\{\sqrt{2}\,\mathrm{Im}\,\rho^2_{10}\sin 2\Theta\sin\Phi+\mathrm{Im}\,\rho^2_{1-1}\sin^2\Theta\sin 2\Phi\},$$

$$\mathcal{W}^3(\cos\Theta,\Phi)=\frac{3}{4\pi}\{\sqrt{2}\,\mathrm{Im}\,\rho^3_{10}\sin 2\Theta\sin\Phi+\mathrm{Im}\,\rho^3_{1-1}\sin^2\Theta\sin 2\Phi\}. \tag{A18}$$

We now present the formula for the cases where only the incoming photon is polarized. The decay angular distributions for the various photon polarizations can be expressed in terms of the above ''partial'' distributions by appropriately specifying the components P^α_γ of the vector $\mathbf{P}_\gamma$ of Eq. (A8) in Eq. (A14).

Unpolarized photons. Obviously, we have

$$\mathcal{W}_{\mathrm{unpol}}(\cos\Theta,\Phi)=\mathcal{W}^0(\cos\Theta,\phi). \tag{A19}$$

Circularly polarized photons of helicity $\lambda_\gamma=\pm1$. By using Eq. (A9) to define P^α_γ, we have

$$\mathcal{W}^{\pm}=\mathcal{W}^0(\cos\Theta,\Phi)\pm P_\gamma\mathcal{W}^3(\cos\Theta,\Phi). \quad \text{(A20)}$$

Linearly polarized photons. By using Eq. (A10) to define P_γ^α, we have

$$\mathcal{W}^L(\cos\Theta,\Phi,\psi)=\mathcal{W}^0(\cos\Theta,\phi) - P_\gamma\cos 2\psi\mathcal{W}^1(\cos\Theta,\Phi) - P_\gamma\sin 2\psi\mathcal{W}^2(\cos\Theta,\Phi). \quad \text{(A21)}$$

By using Eqs. (A17)–(A21), one can see that different density matrix elements $\rho^\alpha_{\lambda,\lambda'}$ have definite physical meaning and may be directly extracted from the data. To see some useful examples, let us define the azimuthal angle-averaged angular distribution functions

$$\overline{\mathcal{W}}^\alpha(\Theta)=\frac{1}{2\pi}\int\mathcal{W}^\alpha(\cos\Theta,\Phi)d\Phi. \quad \text{(A22)}$$

By appropriately combining the data of angular distributions at various angles, we can extract the following density matrix elements:

ρ^0_{00}:

$$\rho^0_{00}=\frac{B^{K^+K^-}+1}{3+B^{K^+K^-}}, \quad \text{(A23)}$$

where

$$B^{K^+K^-}=\frac{\overline{\mathcal{W}}^0(\Theta=0)-\overline{\mathcal{W}}^0(\Theta=\pi/2)}{\overline{\mathcal{W}}(\Theta=\pi/2)}. \quad \text{(A24)}$$

$\mathrm{Re}\,\rho^0_{10}$:

$$\mathrm{Re}\,\rho^0_{10}=\frac{4\pi}{3}\left[\overline{\mathcal{W}}^0\left(\Theta=\frac{\pi}{4}\right)-\mathcal{W}^0\left(\Theta=\frac{\pi}{4},\Phi=\frac{\pi}{4}\right)\right]. \quad \text{(A25)}$$

$\mathrm{Re}\,\rho^0_{1-1}$:

$$\mathrm{Re}\,\rho^0_{1-1}=\frac{4\pi}{3}\left[\overline{\mathcal{W}}^0\left(\Theta=\frac{\pi}{2}\right)-\mathcal{W}^0\left(\Theta=\frac{\pi}{2},\Phi=\frac{\pi}{2}\right)\right]. \quad \text{(A26)}$$

ρ^1_{00}:

$$\rho^1_{00}=\frac{4\pi}{3}\left[\overline{\mathcal{W}}^L\left(\Theta=0,\psi=\frac{\pi}{2}\right)-\overline{\mathcal{W}}^L(\Theta=0,\psi=0)\right]. \quad \text{(A27)}$$

ρ^1_{11}:

$$\rho^1_{11}=\frac{4\pi}{3}\left[\overline{\mathcal{W}}^L\left(\Theta=\frac{\pi}{2},\psi=\frac{\pi}{2}\right)-\overline{\mathcal{W}}^L\left(\Theta=\frac{\pi}{2},\psi=0\right)\right]. \quad \text{(A28)}$$

ρ^1_{1-1}. This density matrix element is related to the asymmetry of linearly polarized photons:

$$\Sigma_\phi\equiv\frac{\sigma_\parallel-\sigma_\perp}{\sigma_\parallel+\sigma_\perp}=\frac{1}{P_\gamma}\,\frac{\mathcal{W}^L(\Theta=\pi/2,\Phi=\pi/2,\psi=\pi/2)-\mathcal{W}^L(\Theta=\pi/2,\Phi=\pi/2,\psi=0)}{\mathcal{W}^L(\Theta=\pi/2,\Phi=\pi/2,\psi=\pi/2)+\mathcal{W}^L(\Theta=\pi/2,\Phi=\pi/2,\psi=0)}, \quad \text{(A29)}$$

where $\sigma_\parallel$ and $\sigma_\perp$ are the cross sections for symmetrical K^+K^- pairs produced parallel and normal to the photon polarization plane, respectively; namely $\sigma_\parallel$ ($\sigma_\perp$) is evaluated by setting $\psi=\pi/2$ (0) in Eq. (A21). By using Eqs. (A17), (A18), and (A21) to evaluate Eq. (A28), we find that

$$\Sigma_\phi=\frac{\rho^1_{11}+\rho^1_{1-1}}{\rho^0_{11}+\rho^0_{1-1}}. \quad \text{(A30)}$$

With the determination of ρ^1_{11} by using Eq. (A28), $\rho^1_{a,-1}$ can then be extracted from Eq. (A30).

We now turn to a discussion of how to use the extracted density matrices to identify the underlying reaction mechanisms. To illustrate this, let us consider the diffractive Pomeron ($P_{1,2}$) exchange and pseudoscalar (PSE) exchange amplitudes at $\theta\simeq 0$. In Sec. III it is shown that

$$T^{P_{1,2}}_{\lambda_f\lambda;\lambda_i\lambda_\gamma}(\theta=0)=T_0^{P_{1,2}}\delta_{\lambda_i\lambda_f}\delta_{\lambda_\gamma\lambda} \quad \text{(A31)}$$

$$T^{\mathrm{PSE}}_{\lambda_f\lambda;\lambda_i\lambda_\gamma}(\theta=0)=T_0^{\mathrm{PSE}}(-1)^{\lambda_\gamma+2\lambda_i}\delta_{\lambda_i\lambda_f}\delta_{\lambda_\gamma\lambda}. \quad \text{(A32)}$$

The phase factor in Eq. (A32) is due to the nature of the pseudoscalar coupling of a boson with a fermion. By using the above helicity conserving amplitudes, the density matrices defined in Eq. (A13) takes the following simple forms:

$$\rho^0=\begin{pmatrix}\frac{1}{2}&0&0\\0&0&0\\0&0&\frac{1}{2}\end{pmatrix},\quad \rho^3=\begin{pmatrix}\frac{1}{2}&0&0\\0&0&0\\0&0&-\frac{1}{2}\end{pmatrix},$$

$$\rho^1=\begin{pmatrix}0&0&\pm\frac{1}{2}\\0&0&0\\\pm\frac{1}{2}&0&0\end{pmatrix},\quad \rho^2=-i\begin{pmatrix}0&0&\pm\frac{1}{2}\\0&0&0\\\mp\frac{1}{2}&0&0\end{pmatrix}, \quad \text{(A33)}$$

where the upper (lower) sign in $\rho^{1,2}$ corresponds to $P_{1,2}$ (PSE) amplitudes. By using Eq. (A33), we then have a very definite prediction for the $\phi\to K^+K^-$ decay asymmetry of Eq. (A30):

$$\Sigma_{\phi}^{P_{1,2}}=+1$$

and

$$\Sigma_{\phi}^{\mathrm{PSE}}=-1.$$

The above results can be generalized to characterize the reaction mechanisms in the t channel. In general, we can decompose the total amplitude as a sum of the natural and unnatural parity exchange parts

$$T=T^{N}+T^{U}, \tag{A34}$$

where

$$T^{N/U}(\theta)_{\lambda_f\lambda;\lambda_i\lambda_\gamma}=\frac{1}{2}\{T(\theta)_{\lambda_f\lambda;\lambda_i\lambda_\gamma} \mp(-1)^{\lambda}T(\theta)_{\lambda_f-\lambda_\phi;\lambda_i-\lambda_\gamma}\}. \tag{A35}$$

By using Eqs. (A31) and (A32), we obviously for our example have $T^{\mathrm{P,SE}}=T^{N}$, $T^{\mathrm{PSE}}=T^{U}$.

We can also define the density matrices for particular parity exchanges. For example, it is useful to consider

$$\rho^{0(N/U)}_{\lambda\lambda'}=\frac{1}{2}[\rho^{0}_{\lambda\lambda'}\mp(-1)^{\lambda}\rho^{1}_{-\lambda\lambda'}]. \tag{A36}$$

By using Eqs. (A19) and (A17), we can use the above density matrix to define the total cross sections σ^{N} and σ^{U} due to the natural and unnatural parity exchange. The parity asymmetry is then defined as

$$P_{\sigma}\equiv\frac{\sigma^{N}-\sigma^{U}}{\sigma^{N}+\sigma^{U}}=2\rho^{1}_{1-1}-\rho^{1}_{00}. \tag{A37}$$

We see that the ρ^{1}_{1-1} and ρ^{1}_{00} extracted by using Eqs. (A26)–(A29) can be used to measure the relative importance between the natural and unnatural parity exchange mechanisms.

The Pomeron exchange (and scalar-meson exchange) is a natural parity exchange process, while the pseudoscalar meson exchange is a unnatural parity exchange process. These two processes have a further simplification that the helicity is conserved, as defined in Eqs. (A31), (A32). By using Eqs. (A32) and (A36), we therefore have the following simple results:

$$\Sigma_{\phi}=P_{\sigma}=\pm 1. \tag{A38}$$

By using Eqs. (A32) and (A19)–(A21), we obtain the following simple forms of the angular distributions.

Unpolarized photons.

$$\mathcal{W}_{\mathrm{unpol}}(\cos\Theta,\Phi)=\frac{3}{8\pi}\sin^{2}\Theta. \tag{A39}$$

Circularly polarized photons of helicity $\lambda_\gamma=\pm 1$.

$$\mathcal{W}^{\pm}(\cos\Theta,\Phi)=\frac{3}{8\pi}\sin^{2}\Theta\pm P_{\gamma}\times 0. \tag{A40}$$

Linearly polarized photons.

$$\mathcal{W}^{L}(\cos\Theta,\Phi,\psi)=\frac{3}{8\pi}\sin^{2}\Theta\{1\pm P_{\gamma}\cos[2(\Phi-\psi)]\}. \tag{A41}$$

In the above equations plus (minus) corresponds to natural (unnatural) parity exchange.

2. Choice of the decay reference frame

The different decay frames discussed in the literature are depicted in Fig. 2(b), and as we mentioned above, it is difficult to give advantage to one prior to another. Some qualitative consideration is in favor of the Gottfried-Jackson (GJ) system, because certain of amplitudes take a simple form here, similar to Eqs. (A31), (A32), but for arbitrary θ. That is, for example, t-channel amplitudes with effective scalar (pseudoscalar) exchanges. In this case the helicity amplitude is factorized

$$T_{if}=[W^{B}_{kl}\varepsilon^{k}_{\lambda_\phi}\varepsilon^{l}_{\lambda_\gamma}]\cdot[W^{F}_{\lambda_f,\lambda_i}], \tag{A42}$$

where the first term depends on the γ-ϕ helicities, and the second one on the fermion spin degrees. In the ϕ-rest system with $\mathbf{q}=0$, the boson part may depends only on two scalar combinations

$$M_{\phi}E_{\gamma}\boldsymbol{\varepsilon}_{\lambda_\phi}\cdot\boldsymbol{\varepsilon}_{\lambda_\gamma},\quad iM_{\phi}\boldsymbol{\varepsilon}_{\lambda_\phi}\cdot[\boldsymbol{k}_{\gamma}\times\boldsymbol{\varepsilon}_{\lambda_\gamma}]=\lambda_{\gamma}M_{\phi}E_{\gamma}\boldsymbol{\varepsilon}_{\lambda_\phi}\cdot\boldsymbol{\varepsilon}_{\lambda_\gamma}, \tag{A43}$$

corresponding to the scalar and pseudoscalar exchange, respectively. So, the dependence of the amplitudes on the γ-ϕ helicities takes the form

$$T_{\lambda_\phi\lambda_\gamma}\sim W_{0}\boldsymbol{\varepsilon}_{\lambda_\phi}\cdot\boldsymbol{\varepsilon}_{\lambda_\gamma}, \tag{A44}$$

and it is different in the different frames, following the scalar product $\boldsymbol{\varepsilon}_{\lambda_\phi}\cdot\boldsymbol{\varepsilon}_{\lambda_\gamma}$.

Helicity system:

$$\boldsymbol{\varepsilon}_{\lambda_\phi}\cdot\boldsymbol{\varepsilon}_{\lambda_\gamma}=d^{1}_{\lambda_\gamma\lambda_\phi}(\chi),\quad \chi=\mathrm{a}\cos\left(\frac{\cos\theta-u_{\phi}}{1-u_{\phi}\cos\theta}\right), \tag{A45}$$

where u_ϕ is the velocity of ϕ in the c.m.s.

Adair system:

$$\boldsymbol{\varepsilon}_{\lambda_\phi}\cdot\boldsymbol{\varepsilon}_{\lambda_\gamma}=d^{1}_{\lambda_\gamma\lambda_\phi}(\theta). \tag{A46}$$

Gottfried Jackson system:

$$\boldsymbol{\varepsilon}_{\lambda_\phi}\cdot\boldsymbol{\varepsilon}_{\lambda_\gamma}=\delta_{\lambda_\gamma\lambda_\phi}. \tag{A47}$$

So, only in the GJ system has the amplitude of Eq. (A42) have a ''helicity conserving'' form for arbitrary ϕ production angle and the corresponding density matrices have the form of Eq. (A33) with the constant matrix elements. In other systems we get additional ''kinematical'' dependence

on θ. That is the reason why the GJ system is preferable. But let us emphasize, that in the real case the total amplitude is the coherent sum of the different terms with their own symmetry and generally, it cannot be factorized in the form of Eq. (A42), therefore, the corresponding density matrices have more complicated form as compared with Eq. (A33), with their specific θ dependence.

The helicity amplitude in the GJ system is related to the amplitude in the c.m.s. by the Wigner rotation

$$T^{\rm CM}_{\lambda_f\lambda_\phi;\lambda_i\lambda_\gamma}=\sum_{l,m} T^{\rm GJ}_{\lambda_f l;m\lambda_\gamma} d^1_{l\lambda}(\omega_\phi) d^{1/2}_{m\lambda_i}(\omega_p),$$

$$T^{\rm GJ}_{\lambda_f\lambda_\phi;\lambda_i\lambda_\gamma}=\sum_{l,m} T^{\rm CM}_{\lambda_f l;m\lambda_\gamma} d^1_{l\lambda}(-\omega_\phi) d^{1/2}_{m\lambda_i}(-\omega_p), \tag{A48}$$

where the corresponding Wigner rotating angles read

$$\omega_\phi=\chi,$$
$$\omega_p={\rm a\,tan}\frac{u_\phi \sin(\pi-\theta)(1-v_p^2)^{1/2}}{v_p+u_\phi\cos(\pi-\theta)}, \tag{A49}$$

where v_p is the proton velocity in the c.m.s.

APPENDIX B: PHASES OF $\phi\to\gamma\pi$

We assume that the $\phi\to\gamma\pi$ decay is dominated by the nonideal ϕ-ω mixing

$$\omega=\omega_8\cos\theta_V+\omega_1\sin\theta_V,$$
$$-\phi=-\omega_8\sin\theta_V+\omega_1\cos\theta_V,$$
$$\omega_1=\frac{1}{\sqrt{3}}(u\bar{u}+d\bar{d}+s\bar{s}),\quad \omega_8=\frac{1}{\sqrt{6}}(u\bar{u}+d\bar{d}-2s\bar{s}), \tag{B1}$$

where θ_V is the ϕ-ω mixing angle: $\theta_V={\rm a\,tan}\sqrt{2}-\Delta\theta_V$, with $\Delta\theta_V\simeq 3.4°$, and for ideal mixing $\phi_0=-s\bar{s}, \omega_0=(1/\sqrt{2})(u\bar{u}+d\bar{d})$. That gives

$$\frac{\phi\to\gamma\pi}{\omega\to\gamma\pi}=-\tan\Delta\theta_V. \tag{B2}$$

The ratio for the amplitudes of the $\phi\to\gamma\eta$ and $\omega\to\gamma\eta$ decays one can obtain in the quark model [57], assuming the flavor structure of π^0 mesons as

$$\pi^0=\frac{1}{\sqrt{2}}(u\bar{u}-d\bar{d}), \tag{B3}$$

one obtains

$$\frac{\phi\to\gamma\eta}{\omega\to\gamma\pi}\simeq\frac{\phi_0\to\gamma\eta}{\omega_0\to\gamma\pi}=-\frac{2}{3\sqrt{3}}(\sqrt{2}\cos\theta_\eta+\sin\theta_\eta)\simeq -0.48$$
$$<0, \tag{B4}$$

for the η-η' mixing angle θ_η around $-10°$ [36]. Considering that the positive sign of $g_{\omega\gamma\pi}$ is known from pion photoproduction [55,56] we get

$$g_{\phi\gamma\pi}=-0.141,\quad g_{\phi\gamma\eta}=-0.707. \tag{B5}$$

Note that sometimes one can find another convention for the meson quark structure with $\pi^0,\rho^0=(d\bar{d}-u\bar{u})/\sqrt{2}$ (see Refs. [57,58]) which leads to the opposite sign of the $\phi\to\gamma\pi$ coupling. Taking into account the importance of fixing the relative phases for our consideration and in order to avoid this ambiguity we make an independent checking of them using symmetry properties of the unitary meson multiplets.

The effective Lagrangian for VPA interaction, where V,P,A are the vector meson, pseudoscalar (π^0,η), and electromagnetic fields, respectively, reads

$$\mathcal{L}=\mathcal{L}_1+\mathcal{L}_8,$$
$$\mathcal{L}_1=R_1\varepsilon_{\mu\nu\alpha\beta}\,{\rm Tr}(\nabla^\mu\hat{A}^\nu,\nabla^\alpha P)V_1^\beta,$$
$$\mathcal{L}_8=\sqrt{2}R_8[\varepsilon_{\mu\nu\alpha\beta}\,{\rm Tr}(\{\nabla^\mu V_8^\nu,\hat{A}^\alpha\}\nabla^\beta P)$$
$$+\varepsilon_{\mu\alpha\nu\beta}\,{\rm Tr}(\{\nabla^\mu\hat{A}^\nu,V_8^\alpha\}\nabla^\beta P)], \tag{B6}$$

where

$$\hat{A}^\mu={\rm diag}(2/3,-1/3,-1/3)A^\mu,$$
$$V_1^\mu={\rm diag}(1,1,1)\omega_1^\mu,$$
$$V_8=\begin{pmatrix}\rho^0/\sqrt{2}+\omega_8/\sqrt{6} & \rho^+ & K^{*+}\\ \rho^- & -\rho^0/\sqrt{2}+\omega_8/\sqrt{6} & K^{*0}\\ K^{*-} & \bar{K}^{*0} & -2\omega_8/\sqrt{6}\end{pmatrix},$$
$$P=\begin{pmatrix}\pi^0/\sqrt{2}+\eta_8/\sqrt{6} & \pi^+ & K^+\\ \pi^- & -\pi^0/\sqrt{2}+\eta_8/\sqrt{6} & K^0\\ K^- & \bar{K}^0 & -2\eta_8/\sqrt{6}\end{pmatrix}. \tag{B7}$$

Direct calculation of the corresponding traces (B6) for the $\omega\pi\gamma$ interaction results in

$$\mathcal{L}(\omega\pi\gamma)=\mathcal{L}_1(\omega\pi\gamma)+\mathcal{L}_8(\omega\pi\gamma)$$
$$=\frac{1}{\sqrt{2}}\varepsilon_{\alpha\beta\mu\nu}(R_1\omega_1^\alpha+xR_8\omega_8^\alpha)\nabla^\nu A^\mu\nabla^\beta\pi$$
$$=\frac{1}{\sqrt{2}}\varepsilon_{\alpha\beta\mu\nu}\{(-R_1\cos\theta_V+xR_8\sin\theta_V)\phi^\alpha$$
$$+(R_1\sin\theta_V+xR_8\cos\theta_V)\omega^\alpha\}\nabla^\nu A^\mu\nabla^\beta\pi, \tag{B8}$$

with $x=4/\sqrt{3}$, which leads to the ratio

$$\frac{\phi\to\gamma\pi}{\omega\to\gamma\pi}=-\frac{1-z\tan\Delta\theta_V}{\tan\Delta\theta_V+z},\quad z\equiv\frac{4}{\sqrt{3}}\frac{R_8}{R_0}. \tag{B9}$$

Accordingly, for $\omega\eta_8\gamma$ interaction one obtains

$$\begin{aligned}\mathcal{L}(\omega\eta_8\gamma)&=\frac{1}{\sqrt{6}}\varepsilon_{\alpha\beta\mu\nu}(R_1\omega_1^\alpha-xR_8\omega_8^\alpha)\nabla^\nu A^\mu\nabla^\beta\pi\\&=\frac{1}{\sqrt{6}}\varepsilon_{\alpha\beta\mu\nu}\{-(R_1\cos\theta_V+xR_8\sin\theta_V)\phi^\alpha\\&\quad+(R_1\sin\theta_V-xR_8\cos\theta_V)\omega^\alpha\}\nabla^\nu A^\mu\nabla^\beta\pi,\end{aligned} \tag{B10}$$

which results in

$$\frac{\phi\to\gamma\eta}{\omega\to\gamma\pi}\simeq\frac{\phi\to\gamma\eta_8}{\omega\to\gamma\pi}=-\frac{1}{\sqrt{3}}\frac{1+z\tan\Delta\theta_V}{\tan\Delta\theta_V+z}. \tag{B11}$$

One can see that at $R_8/R_0=\sqrt{3/32}\simeq0.31$, Eqs. (B9), (B11) reproduce the result of the quark model. The value $R_8/R_0=0.31$ agrees with $R_8/R_0=0.27$ of Ref. [59], found from analysis of available data of $V\to P\gamma$ decay.

APPENDIX C: PARAMETERS FOR THE SCALAR EXCHANGE AMPLITUDE

We assume that σ, f_0, and a_0 are the member of unitary nonet, that is, a_0 is the isovector, while σ and f_0 are the isoscalar mixtures of $f_{1,8}$ components

$$\begin{aligned}\sigma&=f_8\cos\theta_s+f_1\sin\theta_s,\\-f_0&=-f_8\sin\theta_s+f_1\cos\theta_s,\end{aligned} \tag{C1}$$

where θ_s is the mixing angle and for ''ideal mixture'' $\tan\theta=\sqrt{2}$ and $f_0=-s\bar{s}$. The mixing angle is determined by

$$\sin^2\theta_s=\frac{M_{f_8}^2-M_\sigma^2}{M_{f_0}^2-M_\sigma^2},$$

$$M_8^2=\frac{4}{3}M_\kappa^2-\frac{1}{3}M_{a_0}^2. \tag{C2}$$

Taking $M_\kappa=900$ MeV [47], one obtains $\theta_s=\mathrm{a}\tan\sqrt{2}-\Delta\theta_s$ with $\Delta\theta_s=-3.21°$. Then we can estimate the ratio $\phi\to\gamma S/\rho\to\gamma\sigma$ for $S=\sigma,f_0,a_0$:

$$\begin{aligned}\frac{\phi\to\gamma\sigma}{\rho\to\gamma\sigma}&=-\frac{1}{6}(2\cos\Delta\theta_V\sin\Delta\theta_s+\sin\Delta\theta_V\cos\Delta\theta_s)\\&\simeq1.75\times10^{-2},\end{aligned}$$

$$\frac{\phi\to\gamma f_0}{\rho\to\gamma\sigma}=-\frac{1}{3}\cos\Delta\theta_V(2-\tan\Delta\theta_V\tan\Delta\theta_s)\simeq-0.67,$$

$$\frac{\phi\to\gamma a_0}{\rho\to\gamma\sigma}=-\frac{\sin\Delta\theta_V}{\cos\theta_s}\simeq-5.9\times10^{-2}. \tag{C3}$$

The coupling $g_{\rho\gamma\sigma}$ is found in Ref. [18] from ρ photoproduction: $g_{\rho\gamma\sigma}\simeq2.71$ and it is positive. Using this value, one can get the ϕ decay couplings

$$\begin{aligned}g_{\phi\gamma\sigma}&\simeq0.047,\\g_{\phi\gamma f_0}&\simeq-1.81,\\g_{\phi\gamma a_0}&\simeq-0.16.\end{aligned} \tag{C4}$$

The unitary symmetry allows to estimate the g_{SNN} couplings as well. The effective Lagrangian for SNN interaction reads

$$\begin{aligned}\mathcal{L}_{SNN}&=g_{a_0}\bar{N}Na_0+\sqrt{3}\cos\Delta\theta_s g_8\bar{N}N\sigma\\&\quad-\sqrt{3}\sin\Delta\theta_s g_8\bar{N}Nf_0,\\g_8&=\frac{1}{\sqrt{3}}\frac{3F-D}{F+D}g_{a_0},\end{aligned} \tag{C5}$$

which results in

$$\begin{aligned}g_{a_0NN}&=\frac{F+D}{3F-D\cos\Delta\theta_s}\frac{1}{g_{\sigma NN}},\\g_{f_0NN}&=-\tan\Delta\theta_s g_{\sigma NN}.\end{aligned} \tag{C6}$$

The σNN coupling constant was determined within various meson-exchange models for NN scattering [28] and also for ω photoproduction [18]. Its value is somewhat model dependent. To be consistent with our treatment of πNN vertex (discussed in Sec. III B), we also follow Ref. [18] here and choose $g_{\sigma NN}=\sqrt{8.0\times4\pi}$ (no error was assigned in Ref. [18]). With $F/D=0.575\pm0.016$ [30], we then obtain $g_{a_0NN}=21.7\pm1.5, g_{f_0NN}=0.56$, where the uncertainty of g_{f_0NN} is related to the uncertainty of $g_{\sigma NN}$. For definiteness, we use the central values $g_{a_0NN}=21.7, g_{f_0NN}=0.56$ in all of our calculations.

As in PSE, we assume that the $g_{\phi\gamma S}$, g_{SNN} couplings are dressed by the off-shell form factors. For σ exchange we accept the monopole form factors with $\lambda_{\sigma\phi\gamma}=\lambda_{\sigma NN}=2$ GeV [28]. For the heavy meson we parametrize the product of two form factors directly [19,48]:

$$F(t)=\frac{\Lambda^4}{\Lambda^4+(M_\varphi^2-t)^2}, \tag{C7}$$

with $\Lambda=0.6$ GeV [19]. Note (i) that the relatively small $g_{\phi\gamma a_0}$ is compensated by the large g_{a_0NN} and all amplitudes have the same order of magnitude and (ii) $g_{a_0nn}=-g_{a_0pp}$ which results in isotopic dependence of SE amplitude.

[1] A. Donnachie and P. V. Landshoff, Nucl. Phys. **B244**, 322 (1984); **B267**, 690 (1986).
[2] M. A. Pichowsky and T.-S. H. Lee, Phys. Lett. B **379**, 1 (1996); Phys. Rev. D **56**, 1644 (1997).
[3] A. Donnachie and P. V. Landshoff, Phys. Lett. B **185**, 403 (1987).
[4] P. V. Landshoff and O. Nachtmann, Z. Phys. C **35**, 405 (1987).
[5] A. Donnachie and P. V. Landshoff, Nucl. Phys. **B311**, 509 (1988); Phys. Lett. B **296**, 227 (1992).
[6] J. R. Cudell, Nucl. Phys. **B336**, 1 (1990).
[7] J.-M. Laget and R. Mendez-Galain, Nucl. Phys. **A581**, 397 (1995).
[8] J. R. Cudell and I. Royen, Phys. Lett. B **397**, 317 (1997); A. Hebecker and P. V. Landshoff, *ibid.* **419**, 393 (1998); M. Diehl, DAPNIA/SPhN, CEA/Saclay Report No. DAPNIA/SPhN-98-16, hep-ph/9803296.
[9] S. V. Goloskokov, Phys. Lett. B **315**, 459 (1993).
[10] T. Nakano, H. Toki, and T.-S. H. Lee, letter of intent for LEPS at Spring-8, RCNP, Osaka University, 1998 (unpublished); T. Nakano and H. Toki, in *Proceedings of the International Workshop on Exciting Physics with New Accelerator Facilities*, SPring-8, Hyogo, 1997 (World Scientific, Singapore, 1998), p. 48.
[11] J. Ellis, M. Karliner, D. E. Kharzeev, and M. G. Sapozhnikov, Phys. Lett. B **353**, 319 (1995).
[12] M. P. Locher and Y. Lu, Z. Phys. A **351**, 83 (1996); D. Buzatu and F. M. Lev, Phys. Lett. B **329**, 143 (1994).
[13] J. Gasser, H. Leutwyler, and M.E. Sainio, Phys. Lett. B **253**, 252 (1991).
[14] D. B. Kaplan and A. V. Manohar, Nucl. Phys. **B310**, 527 (1988); R. D. McKeown, Phys. Lett. B **219**, 140 (1989); E. M. Henley, G. Krein, S. J. Pollock, and A. G. Williams, *ibid.* **269**, 31 (1991).
[15] A. I. Titov, Y. Oh, and S. N. Yang, Phys. Rev. Lett. **79**, 1634 (1997).
[16] U.-G. Meissner, V. Mull, J. Speth, and J. W. Van Orden, Phys. Lett. B **408**, 381 (1997).
[17] N. M. Kroll, T. D. Lee, and B. Zumino, Phys. Rev. **157**, 1376 (1967).
[18] B. Friman and M. Soyeur, Nucl. Phys. **A600**, 477 (1996).
[19] R. A. Williams, Phys. Rev. C **57**, 223 (1998).
[20] K. Schilling, P. Seyboth, and G. Wolf, Nucl. Phys. **B15**, 397 (1970).
[21] A. I. Titov, Y. Oh, S. N. Yang, and Morii, Phys. Rev. C **58**, 2429 (1998).
[22] D. G. Cassel *et al.*, Phys. Rev. D **24**, 2787 (1981).
[23] D. W. G. S. Leith, in *Electromagnetic Interactions of Hadrons*, edited by A. Donnachie and G. Shaw (Plenum Press, New York, 1978), Vol. 1, p. 345.
[24] H. Suganuma, S. Sasaki, and H. Toki, Nucl. Phys. **B435**, 207 (1995).
[25] P. Joos *et al.*, Nucl. Phys. **B122**, 365 (1977).
[26] R. Koch and E. Pietarinen, Nucl. Phys. **A336**, 331 (1980).
[27] V. Stoks, R. Timmermans, and J. J. de Swart, Phys. Rev. C **47**, 512 (1993).
[28] R. Brockmann and R. Machleidt, Phys. Rev. C **42**, 1965 (1989); R. Machleidt, Adv. Nucl. Phys. **19**, 189 (1989).
[29] J. J. De Swart, Rev. Mod. Phys. **35**, 916 (1963).
[30] F. E. Close and R. D. Roberts, Phys. Lett. B **316**, 165 (1993).
[31] W. Grein and P. Kroll, Nucl. Phys. **A338**, 332 (1980).
[32] J. Piekarewicz, Phys. Rev. C **48**, 1555 (1993).
[33] T. Hatsuda, Nucl. Phys. **B329**, 376 (1990).
[34] S. Neumeier and M. Kirchbach, nucl-th/9809246.
[35] B. Krusche *et al.*, Phys. Rev. Lett. **74**, 3736 (1995); L. Tiator, C. Bennhold, and S. Kamalov, Nucl. Phys. **A580**, 455 (1994).
[36] C. Caso *et al.*, Particle Data Group, Eur. Phys. J. C **3**, 1 (1998).
[37] A. I. Titov, T.-S. H. Lee, and H. Toki, nucl-th/9812074.
[38] F. F. Close, N. Isgur, and S. Kumano, Nucl. Phys. **B389**, 513 (1993).
[39] M. Rose and N. A. Tornquist, Phys. Rev. Lett. **76**, 1575 (1997).
[40] D. Morgan, Phys. Lett. **51B**, 71 (1974).
[41] R. L. Jaffe, Phys. Rev. D **15**, 281 (1977).
[42] N. N. Achasov, S. A. Devyanin, and G. N. Shestakov, Z. Phys. C **22**, 53 (1984).
[43] J. Weinstein and N. Isgur, Phys. Rev. D **41**, 2236 (1990).
[44] G. Jansen, B. C. Pearce, K. Holinde, and J. Speth, Phys. Rev. D **52**, 2690 (1995).
[45] F. F. Close, Rep. Prog. Phys. **51**, 833 (1988).
[46] D. Morgan and M. R. Pennington, Phys. Rev. D **48**, 5422 (1993); D. Morgan and M. R. Pennington, *ibid.* **48**, 1185 (1993).
[47] J. A Oller, E. Oset, and J. R. Relaes, hep-ph/9804209; J. A. Oller and E. Oset, hep-ph/9809337.
[48] B. C. Piarce and B. K. Jennings, Nucl. Phys. **A528**, 655 (1991).
[49] H. Haberzettl, Phys. Rev. C **56**, 2041 (1997).
[50] H. Haberzettl *et al.*, nucl-th/9804051.
[51] K. Ohta, Phys. Rev. C **40**, 1335 (1989).
[52] H. Ballam *et al.*, Phys. Rev. C **7**, 3150 (1974).
[53] H. Besh *et al.*, Nucl. Phys. **B70**, 257 (1973).
[54] J. Behrend *et al.*, Nucl. Phys. **B144**, 22 (1978).
[55] M. Gari and H. Hyuga, Nucl. Phys. **A264**, 409 (1976).
[56] T. Sato and T.-S. H. Lee, Phys. Rev. C **54**, 2660 (1996).
[57] F. E. Close, *An Introduction to Quarks and Partons* (Academic Press, London, 1979).
[58] N. W. Dean, *Introduction to the Strong Interactions* (Gordon and Breach, New York, 1976).
[59] J. L. Goity and M. J. Musolf, Phys. Rev. C **53**, 399 (1996).